2-1-2017

Nanocomposite formulations for enhanced oil recovery (EOR)

Marwan Yasser Rezk

The American University in Cairo

The Graduate School Nanotechnology Program

Nanocomposite formulations for Enhanced Oil Recovery (EOR)

A Thesis in Nanotechnology

By Marwan Yasser Rezk

Submitted in Partial Fulfillment

of the Requirements

for the Degree of Masters of Science in Nanotechnology

January 2018

ABSTRACT

The energy crisis faced in the past few years by the decreasing oil prices and the restriction of recovering oil by conventional methods has developed a huge barrier. This barrier is the difficulty to recover oil by unconventional methods because of their high operation cost and the high cost of the materials required to achieve a successful operation. The main scope of this work is to investigate several zinc oxide nanocomposite formulations and their effect on enhancing oil recovery by surfactant polymer flooding methods compared to conventional surfactant polymer flooding. Since the investigation showed a good impact of ZnO nanomaterial on natural polymers but not the same on synthetic polymers and due to limited resources and time; it was decided to work on ZnO NPs/surfactant (Zinc Oxide Nanoparticles/ Surfactant) flooding instead during the core flooding phase.

The work in this thesis is divided into three main phases; synthesis and characterization of nanomaterials, chemicals testing (including surfactants and polymers), and core flooding application. It was possible to fabricate reproduciable ZnO and TiO_2 nanostructures. Upon characterization, preferential ZnO nanostructures were selected to undergo further testing. In the second phase, natural and synthetic polymers were tested to evaluate the impact of ZnO on their degradation and viscoelastic properties. The results showed a positive impact on natural polymers but a negative one on synthetic polymers. In addition, since the ZnO nanoparticles is flooded in the form of suspension; it was crucial to test ZnO suspension stability in various surfactants as well as the effect of ZnO NPs on interfacial tension. The results showed that ZnO NPs/SDS (Zinc oxide nanoparticles/ Sodium Dodecyl Sulphate) is the most stable suspension at ZnO concentration of 0.05 weight percent giving the most optimum reduced interfacial tension. Finally, upon the excution of core flooding experiments, the results showed an incremental oil recovery of 8% compared to conventional surfactant flooding.

The thesis of Marwan Yasser Ahmed Rezk was reviewed and approved by the following:

Nageh K. Allam
Associate Professor and Graduate Director
Physics Department
The American University in Cairo
Thesis Advisor
Committee Chair

Attia Mahmoud Attia
Dean, Faculty of Energy and Environmental Engineering
British Universing in Egypt
Thesis Co-Advisor

Ahmed Youssef
Professor
Packing & Packaging Materials Department
National Research Centre
Thesis Co-Advisor

Maher A. El-Sockary
Professor
Egyptian Petroleum Research Institute
External Examiner

Ehab N. El-Sawy
Assistant Professor
Chemistry Department
The American University in Cairo
Internal Examiner

Adel Awad
Professor
Physics Department
Thesis Moderator

*Signatures are on file in the Graduate School.

TABLE OF CONTENTS

LIST OF FIGURES

LIST OF TABLES

ACKNOWLEDGEMENTS

I would like to express my deepest gratitude to my advisor, Dr. Nageh Allam for being a role model to me on the scientific and on the personal level. On the science level, he was always available to guide me in order to develop my skills and experience. On the personal level, I learned a lot from his ethics, humility and dedication. You have been and will always be my Godfather, I owe you a lot.

I would like to thank all my colleagues at Energy Materials Lab (EML) for being very helpful and supportive. They taught me the true meaning of a team-work.

The collaboration and the hosting of Dr. Tannaz Pak from Teesside University is gratefully acknowledged. She kindly provided me with all the facilities she has in her labs to do my last phase of my experimental work. Financial support from The American University in Cairo is also gratefully acknowledged. In addition, I would like to thank and acknowledge the support of the British University in Egypt and Farid Khamis foundation for funding my masters. I can never forget the great inspiration I had from Eng. Mohammed and Serag el Sheikha; they gave me true motivation in my career and academic life.

A special thanks to my AUC friends for their unconditional support especially Omar Zidan, Yasmine El Kashef, Dina Mohsen, and Alaa Faid. I would like to also thank Toni Taylor, Mostafa Hegazay and Mina Milad.

Finally, I would like to thank my parents; my dad has been of a great help to my vision for my career and my mom and brother have always gave me the support I needed. My masters would have been impossible without them.

DEDICATION

“Verily, my Salat (prayer), my sacrifice, my living, and my dying are for Allah, the Lord of the 'Alamin (mankind)”

The Noble Qur’an, Surat Al - An'am, Verse [126]

Chapter 1

Introduction and Scope of the Thesis

1.1. Importance of Enhanced Oil Recovery

It is estimated that the world can have about 150 to 400 years of coal and 40 to 80 years for oil and 60 to 160 years of natural gas . However, increasing the world population and the energy demands of high standard living shortens the time over which fossil fuels can last. In terms of cost, it is clearly observed that the prices of energy are increasing and hydrocarbon energy is depleting. It has been discovered that surfactants and polymers can help to enhance the productivity of oil through enhanced oil recovery in a big branch called surfactant/polymer flooding. Generally, maximizing the recovery factor of producing oil fields has been the target of most operating companies in the oil industry. At current production rates and available applied technology; proved producible oil reserves may last 54 years. However, this number may increase if newly emerging technologues help to cost effectively unlock production contingencies [1]. For the time being, generation of energy using fossile fuels still outweight the generation of energy using renewable as shown in (**Figure 1-1)**. Due to the increase of oil prices and the global need for energy, more innovative ways are required to extract oil from subsurface while reducing operation cost.

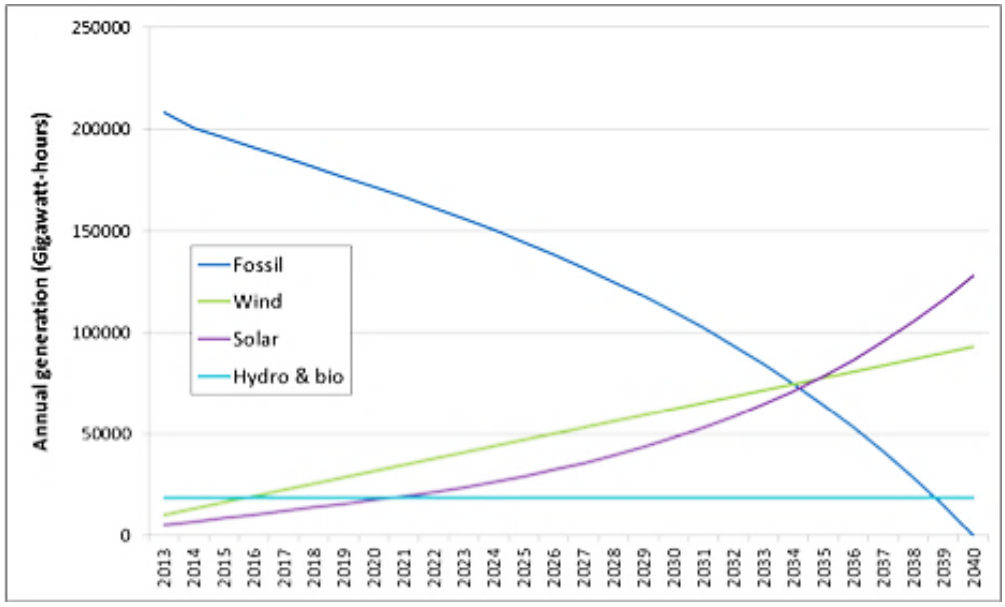

Figure 1 - 1: Annual generation forecast by fossil fuels compared to other renewable energy fuels [2].

Although enhanced oil recovery (commonly called tertiary recovery) offers a solution to extend the life of fossile fuels until renewable energy is fully mature to take over; it is cost ineffective to use enhanced oil recovery methods due to the high prices of chemicals and the huge volumes of chemicals required for successful job. The importance of enhanced oil recovery resides in the plethora of reserve it holds and may produce as shown in (**Figure 1-2**).

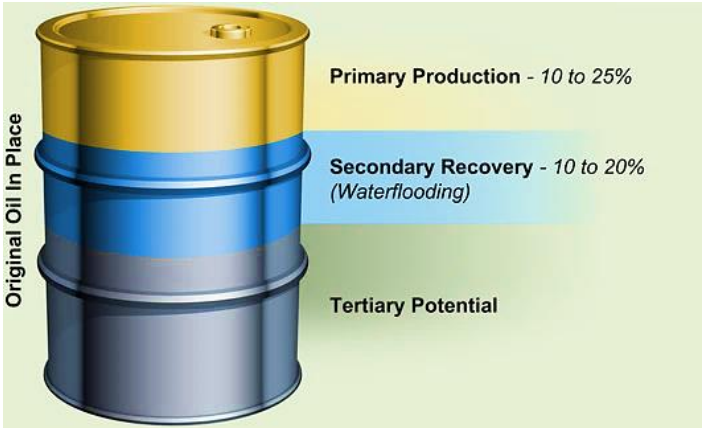

Figure 1 - 2: Tertiary oil recovery potential compared to other recovery methods [3].

There are many enhanced oil recovery methods that can help in oil production. Nevertheless, Frost & Sullivan market research has reported the increasing attention to chemical enhanced oil recovery

is receiving as shown in **(Figure 1-3)**. The figure shows a detailed forecast for the chemicals used in enhanced oil recover and the revenues each may return based on expected usage in market in the form of revenue versus CAGR (Chemical Annual Growth rate).

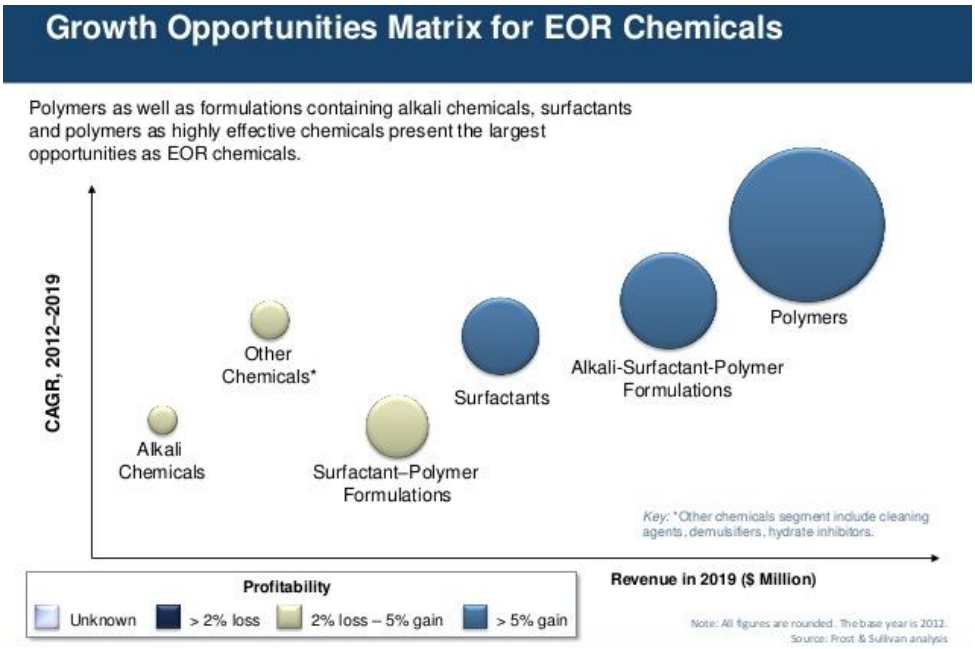

Figure 1 - 3: Importance of surfactants and polymers in chemical enhanced oil recovery [4].

1.2. Chemical enhanced oil recovery challenges

As previously mentioned, the major challenges the chemical enhanced oil recovery is facing are the chemicals cost and the chemicals' limitations. In addition, there are other technical challenges currently facing the use of polymers and surfactants. During the primary and secondary phase of oil recovery, water from aquifer starts trapping oil droplets within the pore spaces due to the water's higher mobility as shown in (**Figure 1-4**). The main target of using polymers and/or surfactants is to alter displacing fluid's viscosity and /or reduce interfacial tension between oil and water to produce trapped oil [5, 6].

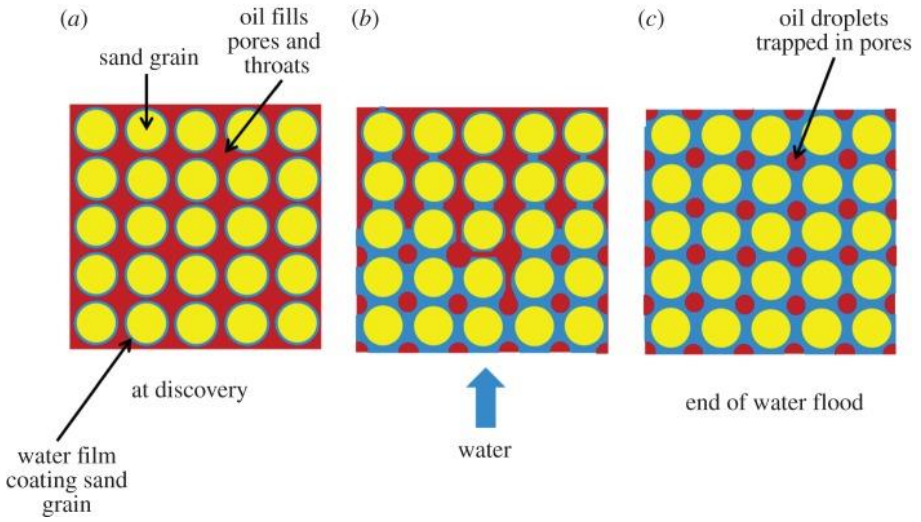

Figure 1 - 4: Oil entrapment by water in water-wet rock [7].

Different polymers are used to achieve favorable mobility where oil can be produced under a piston like behavior that keeps water from trapping oil. However, all polymers are vulnerable to degradation either thermally (natural polymers), mechanically, or chemically (synthetic polymers) [8-10]. Depending on the type of polymer and other conditions, some polymers may get thermally degraded at temperatures as low as 70 ºC (natural polymers). Moreover, the shear rate and salinity may also breakdown the polymer's chains especially at shear rates over 1000 s^{-1} [12]. Despite the fact that polymer flooding can recover a considerable amount of oil that may reach 8 % at low additional cost of 8-16 USD per incremental barrel; other technical difficulties may still restrict the ease of using such technology [13, 14]. For instance, large volumes of polymers are required to achieve a successful field operation to produce a significant amount of oil. In addition, the fact that the polymer is supplied in a powder form to be dissolved later in the rig site may shape a problem in offshore fields where space is limited for such operations.

Surfactants face several challenges in the flooding process that may limit their usage in some fields nowadays or limit their usage in the future due to high cost. Among these challenges are reservoir formation type, and formation salinity. In order to use surfactant in a flooding process on its own or

along with polymer, the clay content in the formation must be small. This can be attributed to the high adsorption of surfactant caused by clays [15]. The adsorption of surfactants makes the amount reaching the target zone (oil bearing formation) less and thus not fulfilling the aimed effect. Otherwise, additional surfactant would be used to make up for the adsorbed (lost) amount which creates extra cost. All the previously mentioned constraints have not limited the usage of surfactants or polymers at different countries [16-18]. However, such limitations have eliminated their usage in some huge fields with significant residual oil saturation [19-21]. It can be fairly acceptable to spend more when there is a good profit margin. As the oil prices are going down nowadays; such contingencies might limit the usage of such polymers or surfactants. Subsequently, it would be highly desired to get ride such limitations to reduce cost or increase efficiency which would be the scope of this work.

1.3. Scope and Objectives of the Thesis

As it will be explained in chapter 2, in some cases both surfactants and polymers (natural or synthetic) have been used to enhance oil recovery in what is called tertiary/enhanced oil recovery.

The performance of most enhanced oil recovery processes depends mainly on three key factors:

1) The effective permeability (K).
2) Viscosity (μ) of the displacing phase with respect to the displaced phase.
3) Reducing interfacial tension.

In the formation, the previously mentioned key factors are manipulated in different ways in favor of oil recovery. One of these ways is surfactant polymer flooding which has been achieving a lot of attention to be developed by nanotechnology. The work done investigated the effect of using ZnO nanocomposite formulations (different nanostructures mixed with surfactants and polymers, each separetely). In addition, the work also investigated the oil recovery enhancement through using ZnO/SDS

formulation in core flooding without using polymers in the injected slug (due to limites resources and time).

Chapter 2 outlines the terminologies mentioned throughout the thesis, including surfactant polymer flooding concepts, mobility control and mobility ratio, and its limitations. It also discusses the basics and importance of surfactants in the oil industry as well as their main role in porous media.

Chapter 3 discusses the relevant literature review of the thesis.

Chapter 4 describes the experimental procedures and conditions used for the preparation and characterization of the studied systems. Nanomaterials and polymers were assessed based on morphology, structure, specific surface area, pH, viscosity, shear rate, and temperature respectively. Chapter 4, also shows a series of stability tests for ZnO at different media including water, polyacrylamide polymer and different surfactant (**SDBS**- Sodium Dodecyl Benzene Sulfonate, **CTAB**- Cetyl Trimethyl Ammonium Bromide, and **SDS**- Sodium Dodecyl Sulfate). In addition, core flooding experiments' conditions and complementary equipment used for it were reported in this chapter.

Chapter 5 presents the results concerning all the experimental work done including characterization and rheology tests for the synthesized nanomaterials and polymers at different concentrations. It also discusses the results concerning the core flood experiments through the NPs/SDS flooding made compared to conventional surfactant flooding.

Chapter 6 highlights the important conclusions from the study and suggests some plans for further work.

References

1. BP 2012. BP statistical review of world energy **2012**. London, UK: BP; See http://www.bp.com/statisticalreview
2. Roberts, D. L. Top 10 Most Interesting Cleantech News Stories from July https://cleantechnica.com/2013/08/06/top-10-most-interesting-clean-tech-news-stories-from-july/.
3. oil recovery overview http://www.midconenergypartners.com/oil-recovery-overview.php
4. Jarosik Follow, A. Emerging Trends in Enhanced Oil Recovery Chemicals Market in the Unit... https://www.slideshare.net/FrostandSullivan/emerging-trends-in-enhanced-oil-recovery-chemicals-market-in-the-united-states-and-europe.
5. Salathiel RA. **1973**. Oil recovery by surface film drainage in mixed-wettability rocks. *J. Petrol. Technol.* 25, 1216–1224
6. Morrow NR. **1990**. Wettability and its effect on oil recovery. *J. Petrol. Technol*. 42, 1476–1484
7. Muggeridge, A.; Cockin, A.; Webb, K.; Frampton, H.; Collins, I.; Moulds, T.; Salino, P. Recovery rates, enhanced oil recovery and technological limits. *Philosophical Transactions of the Royal Society A: Mathematical, Physical and Engineering Sciences* **2013**, 372, 20120320–20120320
8. Clifford, P.; Sorbie, K. The Effects of Chemical Degradation on Polymer Flooding. SPE Oilfield and Geothermal Chemistry Symposium **1985**.
9. Billmeyer, F. W. Textbook of polymer science; *Wiley*: Singapore, **2009**.
10. Carraher, C. E.; Seymour, R. B. Polymer chemistry; M. Dekker: New York, **2003**
11. Seright RS, Seheult M, Talashek T. **2009**. Injectivity characteristics of EOR polymers. *SPE Reservoir Eng. Eval*. 12, 783–792
12. Raney K, Ayirala S, Chin R, Verbeek P. **2012**. Surface and subsurface requirements for successful implementation of offshore chemical enhanced oil recovery. *SPE Prod. Oper*. 27, 294–305

13. Alusta G, Mackay E, Fennema J, Armih K, Collins I. **2012**. EOR vs. infill well drilling: sensitivity to operational and economic parameters. In Proc. North Africa Technical Conf. and Exhibition, Cairo, Egypt, 20–22 February 2012. Tulsa, OK: Society of Petroleum Engineers
14. Sheng, J. J. Status of surfactant EOR technology. *Petroleum* **2015**, 1, 97–105.
15. Morel D, Vert M, Gauchet R, Bouger Y. **2012**. First polymer injection in deep offshore field Angola: recent advances in the Dalia/Camelia field case. *Oil Gas Facilities* 1, 43–52
16. Al-Saadi F, Amri BA, Nofli S, van Wunnik J, Jaspers HF, Harthi S, Shuaili K, Cherukupalli C, Chakravarthi R. **2012**. Polymer flooding in a large field in South Oman—initial results and future plans. In Proc. SP EOR Conf. Oil and Gas West Asia, Muscat, Oman, 16–18 April 2012. Tulsa, OK: Society of Petroleum Engineers.
17. Spildo K, Skauge A, Aarra MG, Tweheyo MT. **2009**. A new polymer application for North Sea reservoirs. *SPE Reservoir Eval. Eng*. 12, 427–432
18. Jayasekera AJ, Goodyear SG. **2002**. Improved hydrocarbon recovery in the United Kingdom Continental Shelf: past, present and future. In Proc. SPE/DOE Improved Oil Recovery Symposium held in Tulsa, OK, 13–17 April 2002. Tulsa, OK: Society of Petroleum Engineers
19. Moulds TP, Trussell P, Haseldonckx SA, Carruthers RA. **2005**. Magnus field: reservoir management in a mature field combining waterflood, EOR and new area developments. In Proc. SPE Offshore Europe Conf., Aberdeen, UK, 6–9 September **2005**. Tulsa, OK: Society of Petroleum Engineers
20. Moulds TP, Trussell P, Erbas D, Cox DJ, Laws ED, Davies C, Strachan N. **2010**. Post-plateau reservoir management in the Magnus field. In Proc. SPE Annu. Technical Conf. and Exhibition, Florence, Italy, 19–22 September 2010. Tulsa, OK: Society of Petroleum Engineers

21. Brodie J, Jhaveri B, Moulds T, Mellemstrand Hetland S. 2012.Review of gas injection projects in BP. In Proc. 18th SPE Improved Oil Recovery Symp., Tulsa, OK, 14–18 April 2012. Tulsa, OK: Society of Petroleum Engineers

Chapter 2

Background

As the demand for oil and gas has been increasing in the past decades using unconventional methods to produce more reserves became very imperative. Naturally, oil can flow normally by natural well pressure which is commonly referred to as primary production. However, as production increases and the amount of fluids decrease in the subsurface, the pressure helping fluids to be produced decreases. At this point, secondary oil recovery is essential to keep the well producing. Usually, secondary recovery utilizes gas/water injection to raise the well's pressure enough to deliver fluids to the surface. Later during this stage, oil production gets very difficult due to various factors rather than pressure. Some of those factors are related to the viscosity of the displacing/displaced phase, interfacial tension, or even permeability. It is pivotal to use enhanced/tertiary oil recovery at this point to overcome such contingencies. Enhanced oil recovery (EOR) is the process of using unconventional techniques such as gas/chemical/thermal energy injection to recover hydrocarbons that cannot be recovered by conventional techniques; EOR is not restricted to a specific phase during the lifetime of a reservoir [1]. The importance of EOR has been highlighted by **(Figure 2-1)** such that shows that the EOR can increase the incremental recovery by 30-70%.

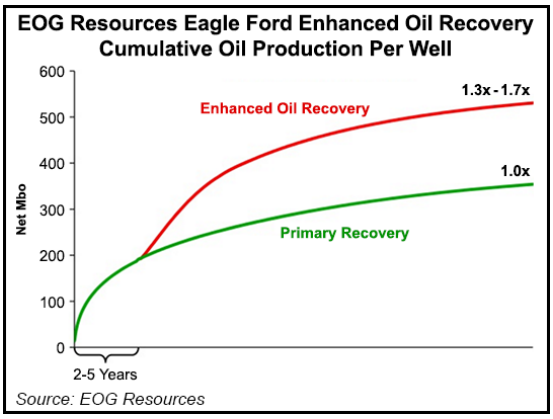

Figure 2 - 1: Importance of EOR based on incremental recovery [2].

EOR has many techniques as previously mentioned; however, the scope of this work will only cover surfactant polymer flooding which is a part of chemical injection. In order to understand well surfactant polymer flooding, it is essential to understand the mechanism of each of them on its own followed by the interaction of both of them together in porous media.

2.1. Polymer flooding

As production goes into the second phase, the water mobility is higher than the oil's mobility as shown in the **(Figure 2-2a)** causing water conning or fingering of aqueous phase in the oil phase. However, using polymer flooding controls the mobility of water with respect to oil's mobility [3]. Applying polymer flooding cause the piston-like mobility behavior shown in **(Figure 2-2b)**.

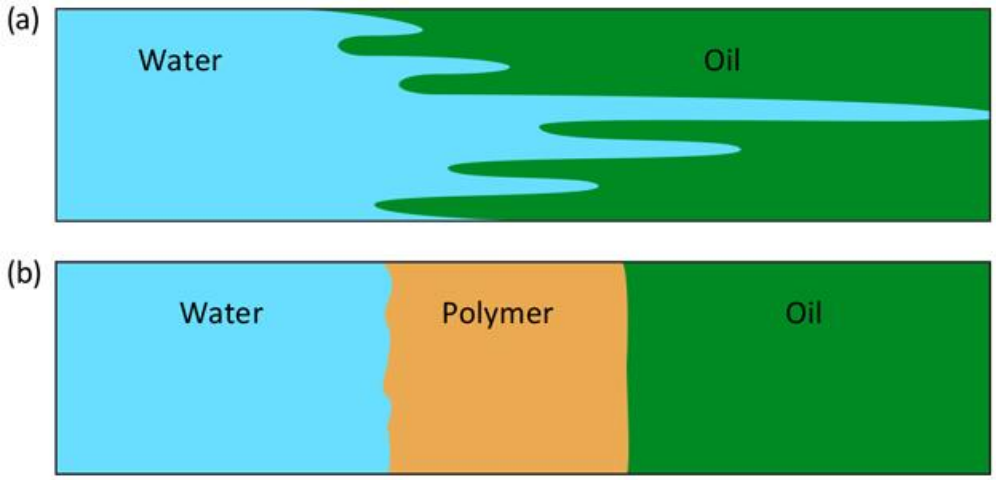

Figure 2 - 2: Polymer flooding piston-like mechanism. (a) Recovery with no polymer. (b) Recovery with polymer [4].

However, the usage of polymer flooding to reduce the displacing phase (water in this case) is utilized to have better control of its mobility with respect to oil (displaced phase). By definition, mobility is the ratio between effective permeability (K) and viscosity (μ) as shown in **(Equation 2.1)**.

$$\lambda = \frac{K}{\mu} \qquad \text{[Equation 2.1]}$$

Changing the permeability parameter with relative permeability (K_r) is the same as changing the whole previous equation to relative mobility equation of a specific phase [5]. But since in the real case more than fluid is encountered in the subsurface; usually, mobility ratio (M_r) is of more interest when dealing with an enhanced oil recovery process. As shown in **(Equation 2.2)** the mobility ratio between the mobility of displacing fluids and the mobility of the displaced fluids should be equal to or less than 1.

$$M_r = \frac{\lambda_{displacing}}{\lambda_{displaced}} \leq 1 \qquad \text{[Equation 2.2]}$$

The two main polymers used in the oil and gas industry to give the previously mentioned effect are synthetic polymers such as polyacrylamide or biopolymers such as Xanthan gum [6]. However, in some rare cases, natural polymers such as Guar gum might be used but they are limited due to their easy thermal degradation compared to synthetic polymers. Zhao in 1991, summarized most important characteristics and structures of a good polymer as shown in **(Table 2-1)**:

Table 2 - 1: Good polymer characteristics candidate for flooding experiments.

Structure	Characteristics	Sample polymer
Carbon chain in the backbone	Gives good thermal stability; slight degradation < 110 C	Polyacrylamide
-O- in the backbone	Gives low thermal stability; severe degradation < 80 C	Carboxymethyl cellulose, Xanthan gum
-COO- in hydrophilic group	It helps for less adsorption on sandstones through good adsorption but gives less chemical stability due to precipitation of Mg^{2+} and Ca^{2+} ions	Sodium alginate, Xanthan gum
-OH or $-CONH_2$ in hydrophilic group	Good Chemical stability but bad viscosity leading to more adsorption on sandstones.	Polyacrylamide, and hydrolyzed polyacrylamide (HPAM)

Thus, as can be concluded from the **(Table 2-1)**, some of the polymer's characteristics are always considered as a challenging matter that flooding project designers have to choose from based on reservoir conditions.

2.2. Polymers history:

Scientists and chemists believed that Mayans were among the first to discover polymers according to the British explorers. They discovered balls made of rubber trees in Central America where the ancient Mayan civilization was located around the 1500s. Later, by the 18th century, Charles Goodyear was the first to discover vulcanization. It is a process by which natural rubber is combined with sulfur and heating them to elevated temperatures to produce vulcanized rubber which is a polymeric substance that is more durable than the natural rubber and it is used nowadays in the car's tires. During the 19th and the 20th century, there has been a huge breakthrough in the field of polymers due to the discovery of the polymerization which opened a huge gate of intense research in several fields. Polystyrene and expanded polystyrene (commonly called styrofoam) were invented by mid 19th century and considered very important polymeric materials used in videocassettes, packaging and thermal packaging [7]. By definition, simply polymer is numerous amounts of chains of repeated units called monomers. The terminology of both monomers and polymers are derived from Greek roots such that mono means one and poly means many [8]. The repeating units could be mainly made up of carbons, hydrogens and sometimes of oxygens, sulfur, nitrogen, chlorine, or fluorine or even others based on the required final polymer. The polymers could be structured differently based on the branching of the chains. Polymers could be linear, branched, cross-linked (commonly due to either radiation or vulcanization), or network structured which looks very close to highly cross-linked structures) [9]. In order for a monomer to develop into a polymer chain with any of the previously mentioned, it has to go through a polymerization technique.

There are mainly four polymerization techniques [10]:

a) Coordination polymerization.

b) Condensation or commonly referred to as step growth polymerization.

c) Copolymerization.

d) Addition polymerization or chain growth polymerization.

2.3. General mechanisms of polymerization

Generally, all the previously mentioned polymerization techniques are composed of three main stages or steps [11]. Firstly, initiation step, it is the step in which the initiator molecule go through chemical reaction under heat conditions to generate active species. The active species kind or type depends on the polymerization technique such that the active species could be a free radical (radical polymerization/chain growth polymerization), an acid (cationic polymerization/ chain growth polymerization), nucleophile (anionic polymerization/ chain growth polymerization) or a transition metal complex (coordination catalytic polymerization/ chain growth polymerization). The active species starts adding to the monomer's carbon-carbon double bond and hence starts polymerization. The monomer used initially becomes the first repetitive unit in the succeeding polymer chain. Secondly, propagation step, it is the step in which every newly generated active species add up to other monomers as previously discussed in the initiation step. Finally, during the termination step, the chain growth usually terminates due to the reaction with another chain or due to the decomposition of the active site. This is the general polymerization in almost all polymers except for ***living polymers.*** Living polymers are polymers that keep propagating to a specific size while chain termination degree is negligible [12]. The only type of polymerization technique that will be encountered in this work is addition polymerization since it is the technique used to polymerize polyacrylamide polymer in this work.

2.3.1. Addition polymerization mechanisms

Addition polymerization is divided into two main classes; it can either happen due to free radical polymerization or ionic polymerization.

2.3.2. Ionic polymerization

Ionic can be categorized into two categories that include cationic and anionic based on the nature of the ions used in the initiation process [6]. Cationic ionic polymerization includes the usage of initiators that provide H^+ ions or positive ions. Such type could be very effective when used with monomers that have groups that release electrons like phenyl ($-C_6H_5$) or methyl ($-CH_3$) groups which include styrene and propylene. Anionic ionic polymerization includes the usage of initiators that can provide negative ions. It is very effective when used with groups that are considered to be electron acceptors such as chloride (-Cl) and nitrile (-CN).

2.3.3. Free radical polymerization

In this type of polymerization, the monomer is polymerized by the means of an initiator that generates free radical that acts as a catalyst [13]. A free radical may be simply defined as uncharged molecule that is highly reactive, has an odd number of electrons and it is not a free ion either.

2.4. Surfactant flooding

Another pivotal process used in EOR is called surfactant flooding. It is mainly concerned with using a surface acting material to reduce the interfacial tension between oil phase and aqueous phase allowing more oil to be recovered. Before going into surfactant's mechanism in porous media; it would be essential to mention the general types of surfactant and their uses in the oil industry [14]. Surfactants are made of head (hydrophilic group) and tail (hydrocarbon chain). The main types of surfactants are anionic (negatively charged head), cationic (positively charged head), nonionic (non-charged end), and

zwitterionic (have both positive and negative charges attached). Anionic surfactants are the most widely used in EOR due to their low adsorption on sandstone because they have similar charges. Nonionic sometimes are mixed along with anionic surfactants to increase resistance to salinity. A very crucial parameter that needs to be in consideration when using surfactants is called critical micelle concentration (CMC). It has been defined as the concentration by which micelles are formed. Oil water systems can benefit in different ways upon introducing surfactants at CMC. Firstly, surfactants would reduce energy at the interface between oil and water. Secondly, the hydrophobic part of the surfactants (tail) doesn't interact with the water and hence as the surface coverage of surfactant increases, the surface free energy decreases. As shown in **(Figure 2-3)** the micelles are formed by increasing the surfactant concentration.

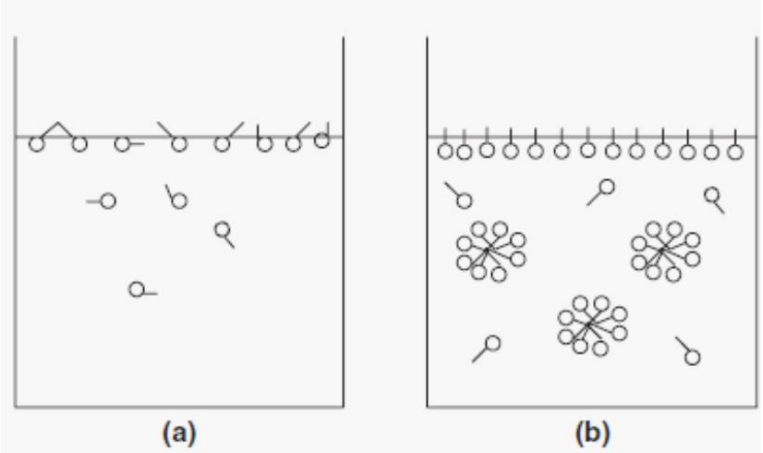

Figure 2 - 3: (a) surfactants behavior below CMC concentration. (b) Micelles formation above CMC formation [15].

Surfactant's CMC concentration is highly related to what is referred to as Krafft temperature. By definition, Krafft temperature is the temperature under which no micelles can be formed regardless of the CMC concentration. In addition, there are other parameters and theories related to the selection of new surfactant for oil recovery application [16]. The most important parameter of these parameters is referred to as solubilization, which is discussed briefly in this chapter. Solubilization ratio can be defined as a ratio of the volume of solubilized oil/water to the volume of surfactant used in the microemulsion phase. Solubilization ratio is a strong indicator for interfacial tension (IFT) reduction. In other words, when the solubilization ratio of oil is close or equal to that of the water's, the IFT reaches the minimum.

Microemulsions are very common when introducing surfactants to oil/water systems. But before introducing the microemulsion types in oil/water systems it is essential to describe the difference between microemulsions and macroemulsions. On one hand, macroemulsions can be described as the mixture of two or more immiscible fluids where one phase is dispersed in another continuous phase. The macroemulsions are usually cloudy in appearance due to the scattering of light as it passes through different phases. On the other hand, microemulsions are transparent and translucent fluids that thermodynamically stable. They tend to have a transparent appearance due to the small size of the dispersed phase.

There are three main types of microemulsion ternary diagrams based on the salinity present in the oil/water system. The three types are shown in **(Figure 2-4)** and explained below.

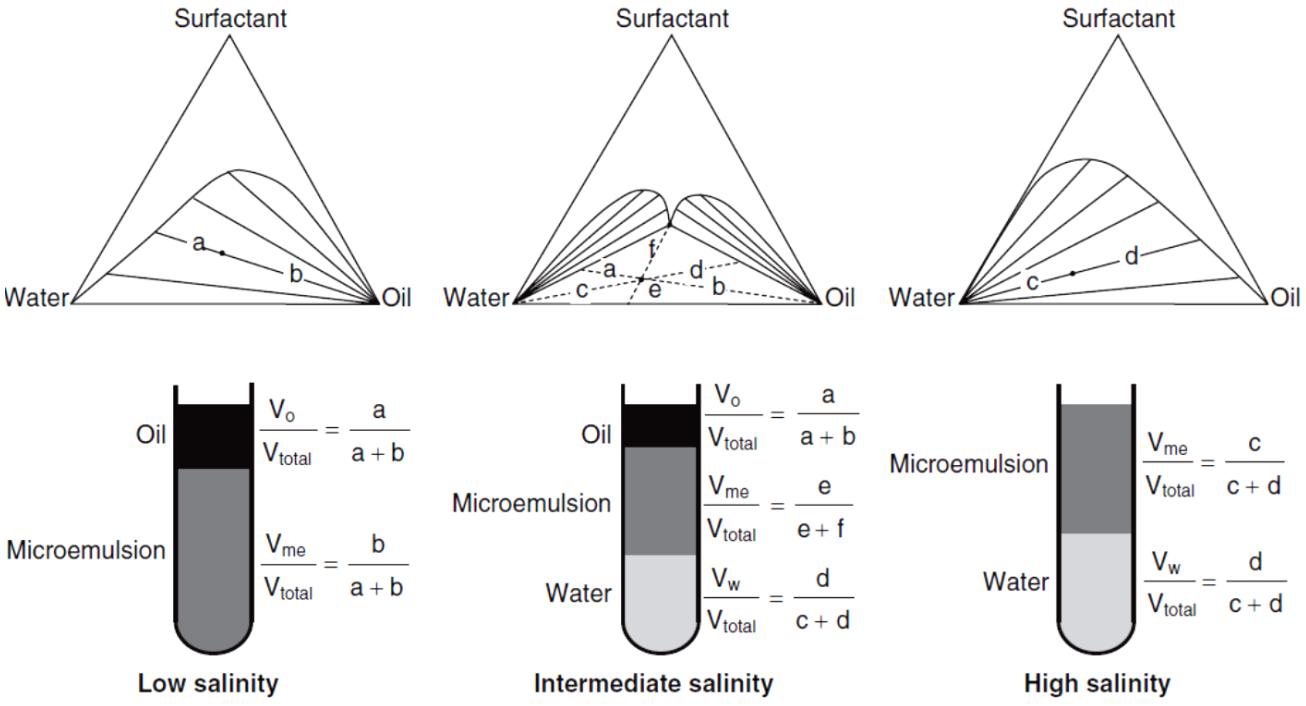

Figure 2 - 4: 3 types of microemulsions in oil/water systems. (Low salinity: type II (-ve)), (Intermediate salinity: type III), (high salinity: type II (+ve)) [15].

Type II (-ve) has two phases; water external microemulsion phase and an oil phase. Since the

microemulsion is composed of aqueous phase it is referred to as a lower phase because it is denser than oil/oleic phase. Type II (+ve) in high salinity, the oil/water system separates into oil-external microemulsion and water phase. The intermediate range of salinity formulates 3 phases system in type III where microemulsion is in between oil and water which usually exhibit the least interfacial tension. The terminology of the different types of microemulsion systems is based on the slope of the tie lines within the microemulsion environment [17].

Although the main scope of this thesis is not to discuss surfactants it is important to mention the displacement mechanism in surfactant (micellar) flooding. Firstly, in type II (-ve) oil present in the reservoir is carried by more dense microemulsion and be produced along with the oil bank. Where in Type II (+ve), it is quite simple for external oil to coalesce with residual oil to form an oil bank that can be produced. Finally, upon the solubilization of oil and water together in type III, few things happen to help the oil recovery. Firstly, oil mobility is enhanced through the pore throats to gather up with more oil to be produced. Secondly, oil and water volumes expand leading to an increase in the relative permeability to oil and water which increase the water cut (production) if not controlled by a viscous mobility controlling agent (polymer) [18].

2.5. Surfactant/polymer flooding

Using polymer along with surfactants in surfactant/micellar-polymer flooding has two main advantages. Firstly, the polymer may cause what is referred to as inaccessible pore volume (IPV) in which big molecules of the polymer does not enter smaller/dead-end pores [19]. This condition promotes polymers to be in the front of the slug and hence promotes a competitive adsorption between polymers and surfactant. In competitive adsorption, more adsorption sites are covered with polymers compared to that covered with surfactants. Secondly, the presence of polymer along with surfactant promotes for mobility control which has been mentioned in the previous paragraph. The order in which the surfactant

and polymer are flooded is usually variable based on the field case. Sometimes, polymers are injected after surfactant to avoid chase water from cause coning or fingering. Other times, polymers are injected before surfactants to act as a sacrificial fluid for adsorption instead of the surfactant itself. And other times they are injected together with the limitation of their compatibility. Many researchers have reported different facts about the interaction of between surfactant and polymer in surfactant polymer flooding [20]. Firstly, although surfactant can exist in any of the three phases mentioned in the ternary diagrams shown in **(Figure 2-4)**, it resides in the most aqueous phase. Secondly, the polymer only affects water-rich phase by increasing its viscosity but doesn't affect the microemulsion phase unless it riches in water. Thirdly, the surfactant can benefit oil production in two different ways either by increasing polymer's viscosity through aggregates formation or by reducing viscosity by bringing cations as Na^+. However, surfactants don't affect PAM and HPAM significantly, because the two effects cancel each other out in such polymers. Fourthly, the viscosity of the hydrophobic polymers can be increased by the addition of surfactants. That was attributed to the solubility of the hydrophobic group of the polymer in the micelles which increase their molecular interaction.

References

1. Donaldson, E. C. Enhanced oil recovery; *Elsevier*: Amsterdam, **1989**
2. Davis, C. EOG Enhancing Eagle Ford Oil Recovery Using Novel NatGas Injection System http://www.naturalgasintel.com/articles/106368-eog-enhancing-eagle-ford-oil-recovery-using-novel-nat
3. Willhite, G. P.; Seright, R. S. Polymer flooding; Society of Petroleum Engineers: Richardson, TX, 2011.
4. Hanssens, O. Recovery from producing fields http://www.npd.no/en/Publications/Resource-Reports/2014/Chapter-2/.
5. Cârcoană, A. Applied enhanced oil recovery; Prentice Hall: Englewood Cliffs, NJ, **1992**.
6. Zhao, F.-L., Chemistry in Oil Production. University of Petroleum, China, **1991**
7. Billmeyer, F. W. Textbook of polymer science; *Wiley*: Singapore, **2009**.
8. Carraher, C. E.; Seymour, R. B. Polymer chemistry; M. Dekker: New York, **2003**
9. Young, R. J.; Lovell, P. A. Introduction to polymers; *CRC Press: Boca Raton*, **2011**
10. Biswas, M. Advances in polymer science; *Springer*: Berlin, **2001**.
11. Su, W.-F. Principles of polymer design and synthesis; Springer-Verlag Berlin An: Place of publication not identified, **2016**.
12. Cantow, H.-J.; DallAsta, G.; Dušek K.; Ferry, J. D.; Fujita, H.; Gordon, M.; Kennedy, J. P.; Kern, W.; Okamura, S.; Overberger, C. G.; et al. Living Polymers and Mechanisms of Anionic Polymerization; Springer Berlin Heidelberg: Berlin, Heidelberg, **1983**.
13. Matyjaszewski, K. Handbook of Radical Polymerization; *John Wiley & Sons*, **2002**.
14. Schramm, L. L. Surfactants: fundamentals and applications in the petroleum industry; Cambridge University Press: Cambridge, U.K., **2000**.

15. Sheng, J. Modern chemical enhanced oil recovery: theory and practice; Gulf Professional: Place of publication not identified, **2016**.
16. Institute, I. I. T. R.; Llave, F. M.; French, T. R.; Lorenz, P. B. Evaluation of mixed surfactants for improved chemical flooding; Department of energy: United states of America, **1993**.
17. Koduru, N. Microemulsion characterization in chemical EOR: an experimental and simulation studies on acidic crudes; **2010**.
18. Healy, R.; Reed, R.; Stenmark, D. Multiphase Microemulsion Systems. *Society of Petroleum Engineers Journal* **1976**, 16, 147–160.
19. Littmann, W. Polymer flooding; *Elsevier*: Amsterdam, **1988**.
20. Norman, A. Surfactant polymer iteraction in enhanced oil recovery; Prairie View A & M University: Texas, United states, **1999**.

Chapter 3

Relevant Literature Review

3.1. Nanomaterials in petroleum engineering

Although the use of nanomaterials have a very high potential, it could be increased if solutions are found for some of the current challenges. The mentioned challenges include relatively high cost, wide differences in effects observed by different researchers, agglomeration, and sedimentation [1]. Various applications for nanomaterials in the petroleum engineering industry have been discussed in the literature [2]. Despite the fact that the application of nanofluids is considered as an emerging technology to the oil industry, several researchers currently are working on optimizing different parameters for the process [3-5]. Recent research studies proved promising application of nanomaterials in oil recovery through mobilizing trapped oil in porous rocks to be produced or through enhancing the mechanism of surfactants/polymers [6]. At the nanoscale, particles behave chemically different from that in the macroscale such that an element might be soluble in water in macroscale but insoluble in water in nanoscale [7]. Several researchers studied and used different nanofluids dispersed in different dispersants in order to use it in oil recovery. Since the stability of nanofluids is a very important parameter for nanofluids to be used in porous media, *Yu and Xie* have reported in 2012 that a suspension will be stable if repulsion forces are greater than attraction forces to avoid aggregation [8]. Researchers have attributed the favorability of using nanofluids to the high surface to volume ratio which increases the diffusion and mass transfer. The previously mentioned explanation can promote nanofluids to reach parts of the oil reservoir that are untouched by normal techniques [9]. Improved oil recovery can be achieved by nanomaterials through different techniques including improving mobility, interfacial tension reduction, and wettability alteration. Because most producing oil reservoirs are sandstones; most successful work has been done using silica nanoparticles due to their surface charge similarity. Silica and sandstone having negative surface charge promote less sedimentation and aggregation of the nanosilica. However,

it is important to mention that other nanomaterials could be used if functionalized to have a compatible surface charge with the rock under experiment.

In 2012, *Oglo et al.* have investigated the effect of different dispersants on different nanomaterials and their effect on oil recovery. Their experimental work involved three main dispersants including distilled water, brine, and ethanol [10]. A wide range of nanomaterials was investigated in that work including alumina, silica, zinc oxide, zirconia, copper oxide, magnesium oxide, iron oxide, and tin oxide. Their results showed that silica and alumina dispersed in brine and ethanol had the highest oil recovery. As briefly discussed above, the oil recovery enhancement could be attributed to wettability alteration, interfacial tension reduction, or improved mobility. Since the main scope of this work is concerned about polymers and surfactants; the use of nanofluids for improved mobility and interfacial tension reduction will be focused upon.

3.2. Nanofluids mobility control

Making use of nanotechnology in the oil field has been a hot research topic in many different ways that includes the recovering oil by directly enhanced conventional mechanisms or enhancing materials. Many researchers have enhanced mobility control through enhancing the polymer's characteristics in order to increase its viscosity. In the mobility control, several researchers have used nano-clay whether to increase viscosity or to enhance resistance factor. According to *Littmann* in 1988, resistance factor can be defined as a ratio between the water's mobility to the polymer's mobility. Additionally, *Rezaei et al.* discussed the previously mentioned results when they used nano-clay with PAM being injected at high salinity condition [11]. They confirmed 33% increase in oil recovery which was attributed to the polymer's enhanced viscosity and enhanced thermal stability. Moreover, *Medhi et al.* in 2017 have used nanoclay to improve the properties of hydrolyzed polyacrylamide and then use it in polymer flooding [12]. The results showed that the nanocomposite had exhibited a higher viscosity in

different shear rates compared to the blank hydrolyzed polyacrylamide even in higher temperatures. It is believed that the nanoclay embedding increases the water uptake of polyacrylamides hence increasing its viscosity. Finally, in the field of nano-metal oxides, Cheraghian have attempted to use titanium dioxide nanoparticles to improve the performance of PAM at different salinities in a sandstone core sample [13]. The results showed 4% oil recovery increase compared to ordinary polyacrylamide with no TiO_2 additives. The results were attributed to improvement in viscosity as well as shear resistance.

3.3. Nanofluids interfacial tension reduction

Commonly, most of the interfacial tension reduction enhancement work done by adding nano-metal oxides to different types of surfactant. Hydrophilic and hydrophobic silica nanoparticles were used at a concentration of 0.1 weight percent along with SDS surfactant in sandstone core samples [14]. The results confirmed more oil recovery due to a reduction in interfacial tension as well as increased adsorption of SDS + silica on the rock surface. Same results were acquired with only hydrophilic silica by *Hendraningrat et al.* but with much fewer nanoparticles concentration. Their results also showed 13% more oil recovery due to interfacial reduction [15]. Other metal oxides have been used in this field as well such as zirconia. The behavior of different surfactants was assessed when used along with a very little concentration of zirconia [16]. The different surfactants included SDS and CTAB surfactant in order to evaluate whether anionic or cationic surfactant would perform better. Surprisingly, both SDS and CTAB showed promising results but for different reasons. Truly, the use of zirconia with SDS showed better results in interfacial tension reduction than that of zirconia with CTAB but the use of zirconia with CTAB showed wettability alteration that did not show with SDS surfactant. Furthermore, it was believed that adding zirconia nanoparticles to the surfactants has modified the flow regime from Newtonian to non-Newtonian which has also increased viscosity almost two times. Other metal oxides have been also investigated to evaluate their effects on surfactant flooding such as titanium dioxide nanoparticles. Using

a glass model, *Cheraghian* proved the success of using titanium dioxide nanoparticles in surfactant flooding to recover heavy oil. His results proved that titanium dioxide could improve oil recovery by 51% [17]. The use of zinc oxide has not been that common except for being used in one publication that did not show good rationale. The publication was, published in 2014, stating that the use of zinc oxide with SDS surfactant may increase oil recovery while increasing interfacial tension [18]. There are many errors during the core flood experiment that may have caused the recovery increase, which would not necessarily be because of interfacial tension increase. In fact, the increase of interfacial tension in porous media having both oil and water makes it impossible to produce oil before water when water has higher mobility.

3.4. Stability of Nanofluids

Stability of nanofluids is a pivotal parameter for the success of nanofluids in enhanced oil recovery applications. The importance of suspension stability is that if the nanomaterials suspended in the solution precipitated they may cause a reduction in porosity as well as permeability. Several researchers have investigated the stability of different nanomaterials in several dispersants with and without stabilizing agents. Furthermore, different methods have been used to assess the stability of a suspension under different conditions.

3.4.1. Stability of ZnO nanoparticles

Zinc oxide has been very useful in the past period for its pros in different fields. Some of the advantages that promote zinc oxide to be used in different fields are low price, anti-corrosive, antibacterial, antifungal properties. In addition, it has a wide band gap that promotes electrons to the conduction band leaving electron holes in the valence band. In 2014, *Fatehah et al.* have investigated the effect of pH on zeta potential by dynamic light scattering technique for ZnO nanoparticles dispersed in deionized water [19]. Through a wide range of pH that goes from 2 to 11 and by adjusting the

suspension's pH using hydrochloric acid (HCl) and sodium hydroxide (NaOH); they were able to report important points about ZnO suspension's stability. Firstly, the concentration of ZnO doesn't affect the overall surface charge over different values of pH. The presence of surface charge can be attributed to either the adsorption of hydroxyls or protons on the surface sites or the deposition of hydroxylated metal species from the solution. The formulated zeta potential profile over the investigated range of pH was reported in **(Figure 3-1)**.

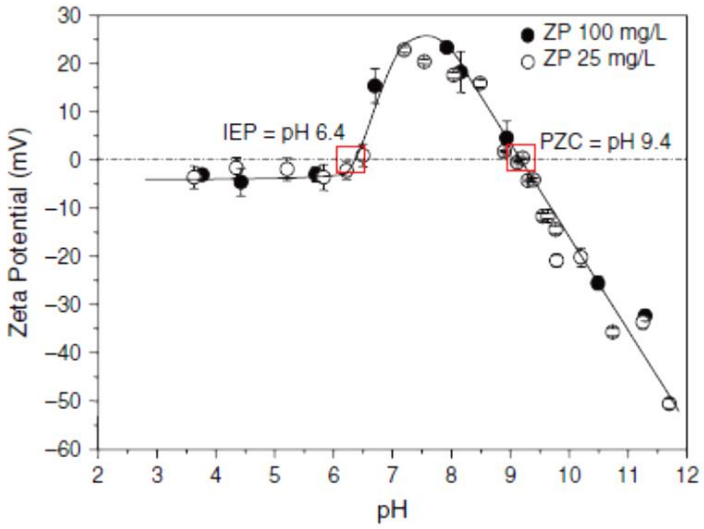

Figure 3 - 1: ZnO NPs in DIW suspension zeta potential profile [19].

The zeta potential profile at the positive, neutral, and negative charge region was attributed to the dominant species at this point of pH. On one hand, in the positive zeta potential region, the dominant species are $Zn^{2+}_{(aq)}$ and Zn $(OH)^{+}_{(aq)}$ions. On the other hand, in the negative zeta potential region, the Zn $(OH)^{-}_{3(aq)}$ and Zn $(OH)^{2-}_{4(aq)}$ determine the overall charge and deposition behavior. While at the point of zero charge (PZC)/isoelectric point (IEP) the $Zn^{2+}_{(aq)}$ and Zn $(OH)^{+}_{(aq)}$ are in equilibrium with surface hydroxide. In addition, *Mudunkotuwa et al.* reported in his thesis a different pH for the point of zero charge (pH = 8.7) [20]. Their results for measuring zeta potential with differing concentrations of citric acid agrees with the previously mentioned work that the positive zeta potential region falls around pH 6.5 – 8.7. They have also used spectrophotometer measurements wavelength 380 nm to assess the

suspension deposition dynamics. However, their work reported a contradicting pH behavior such that the more acidic the suspension is the more negative the surface charge is where the previous work for *Fatehah et al.* proved that the highly negative region falls in basic pH. The results of adding varying concentrations of citric acid to ZnO suspension were reported at **(Table 3-1)**.

Table 3 - 1: Zeta potential of ZnO suspension with varying citric acid concentrations [20].

Citric acid concentration (mM)				
Sample no	0 Zeta potential (mV)	0.3 Zeta potential (mV)	1.0 Zeta potential (mV)	5.0 Zeta potential (mV)
4 nm	+20.7	-19.1	-44.2	-49.7
7 nm	+20.4	-18.0	-23.0	-36.4
15 nm	+15.6	-9.9	-28.3	-40.2

Several researchers have tried to increase the stability of ZnO suspension either by changing the dispersant or by adding surfactants or polymers. Liu et al investigated the effect of different cations to the stability of ZnO suspension stabilized by SDS surfactant [21]. The results showed an exponential decrease in the suspensions' stability when introducing sodium chloride, potassium chloride, and calcium chloride as shown in **(Figure 3-2)**.

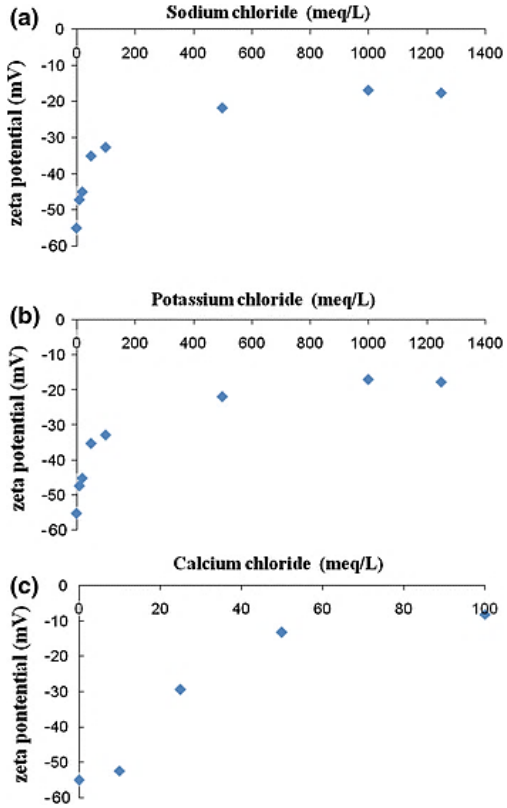

Figure 3 - 2: Effect of different cations on the stability of ZnO suspension stabilized by SDS [21].

The effect observed by cations were attributed to the neutralization of cations to the ZnO surface charge and compression of the electric double layer which promotes aggregation. Other researchers have attempted to investigate the stability of ZnO suspension augmented by polymers. For example, Tang et al have investigated the effect of suspending ZnO NPs in polyethyleneimine (PEI) and measuring zeta potential for it [22]. In the PEI polymer's case, the results proven as shown in **(Figure 3-3)** the polymer's suspension for ZnO NPs is mostly stable in basics pH with a sharp drop in pH 11.5.

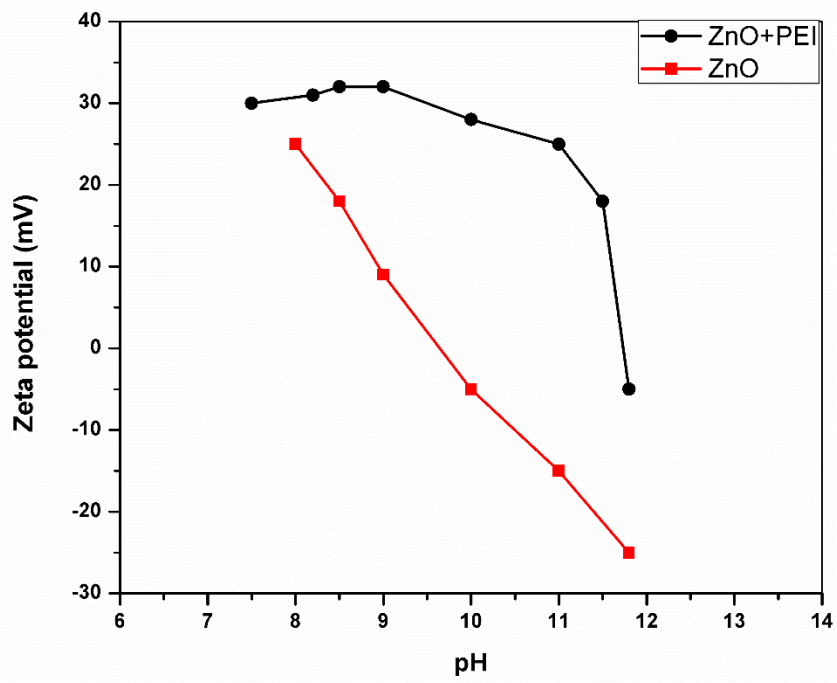

Figure 3 - 3: The effect of PEI on ZnO suspension's zeta potential [22].

The results presented in *Tang's* work were informative about the possibility of using polymers to suspend ZnO in some application where polymers synergistic effects might be required. However, for stability only, a similar stable suspension could be acquired with a negative surface charge without adding PEI.

Finally, some researchers used various surfactants to enhance the stability of ZnO NPs suspensions. *Sadowski and Polowczyk* have attempted to use various surfactant types to suspend different concentrations of ZnO NPs at pH 7.4 - 7.6. Sodium oleate (SOL), (SDS), and (CTAB) [23]. The composed formulations were measured for stability through zeta potential measurement versus surfactant concentration as shown in **(Figure 3-4)**.

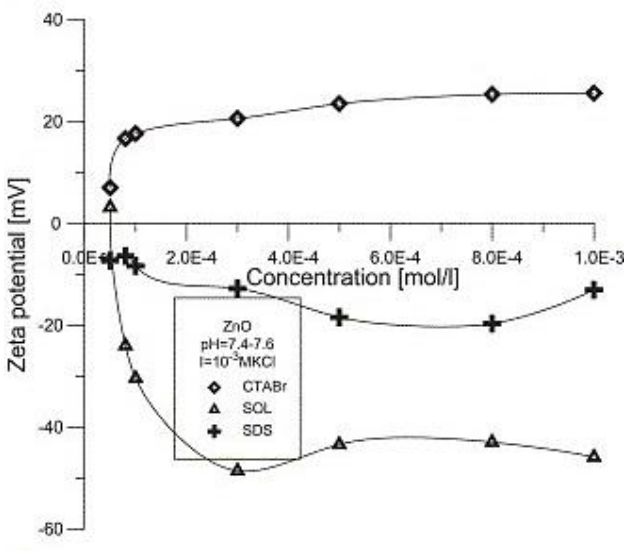

Figure 3 - 4: Stability of ZnO NPs suspensions in different surfactants [23].

The results show that anionic surfactants can have a higher stability than cationic surfactants with negative surface charge. Similarly, *Adil et al.* investigated the effect of several anionic surfactants including SDS, SDBS, and oleic acid at different concentrations on the stability of ZnO [24]. They proved that 0.025 weight percent (slightly above CMC) SDBS can stabilize 0.1 weight percent ZnO when ultrasonicated for 60 min. As shown in **(Figure 3-5)**, 0.025 % SDBS with 0.1 % ZnO shows the longest time for sedimentation at 95 C° and pH 2.

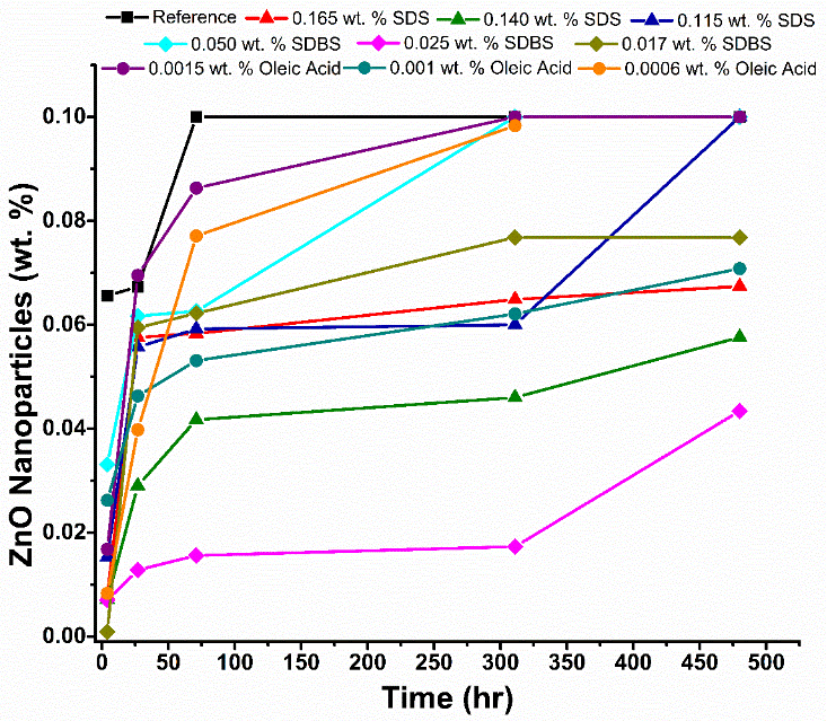

Figure 3 - 5: Sedimentation time for different anionic surfactant + ZnO NPs suspensions [24].

The results were explained in terms of adsorption of free surfactant on dispersed nanoparticles. In other words, due to different charges on ZnO and anionic surfactants; negative ions dissociated from anionic surfactant get adorbed on positively charged ZnO NPs at pH 2 causing neutralization of ZnO particles. Thus, electrostatic stabilization overcomes Van der Waals forces which were better described by the schematic for the particles interaction shown in **(Figure 3-6)**. The mechanism describes an earlier explanation for ZnO nanoparticles interaction with surfactants but in the presence of polymers. The other study discussing polymer, surfactants, and ZnO nanoparticles interaction depended on not only the concentration of surfactant/polymer added to the suspension but also on the order and time of ultrasonication.

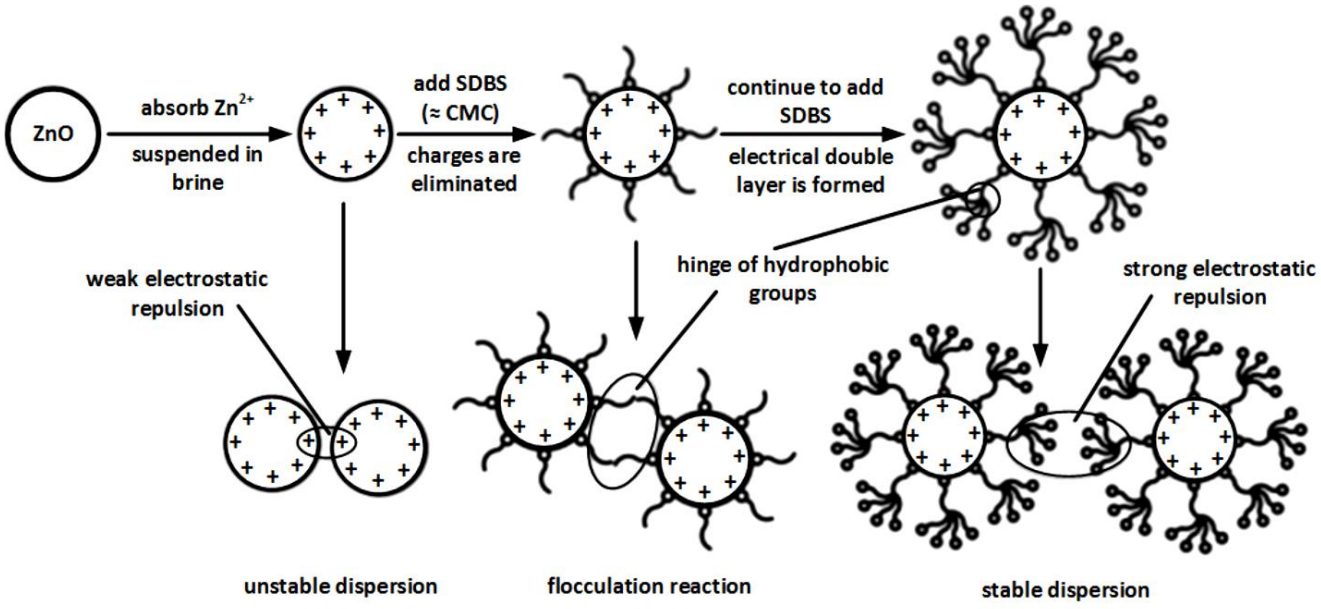

Figure 3 - 6: ZnO NPs interaction with an anionic surfactant [24].

Fiedot et al. have reported and discussed the interaction of surfactants, polymers, and ZnO nanoparticles [25]. They compared the effect of different orders of chemicals added to ZnO nanoparticles. Excess surfactant levels followed by polymers added to ZnO nanoparticles were compared to addition polymers followed by surfactant combined with polymers. The comparison was represented in a schematic shown in **(Figure 3-7)**. On one hand, the first case was explained as when surfactant added first, it will get adsorbed on the nanoparticles interface. Excess surfactant concentration forming micelles will be surrounding the polymers particles instead. On the other hand, when the polymer is firstly introduced, it becomes adsorbed on the surface of the ZnO nanoparticle. Upon the addition of a surfactant, micelles that are surrounded by polymer chains gets attached to the polymer adsorbed on the ZnO nanoparticles causing more compaction of the polymer adsorbed on the nanoparticles. The hypothesis was confirmed by TEM imaging and dynamic light scattering and confirmed the previously discussed structure. In addition, the prolonged stability was attributed to the presence of free micelles that were believed to avoid nanoparticles from combining in larger groups and hence precipitating.

Furthermore, increased surfactant levels reduce surface tension in solution causing a reduced tendency of particles agglomeration.

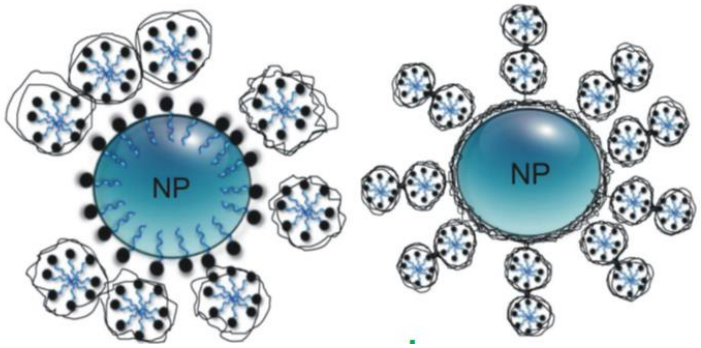

(a) (b)

Figure 3 - 7: (a) Case 1 polymer was used after surfactants. (b) Case 2 polymer introduced to ZnO followed by a mixture of surfactant + polymer [25].

In addition, the use of ZnO nanoparticles in addition to SDS surfactant has been recently investigated with zinc oxide particles size 20 nm [26]. It has been shown that suspending zinc oxide in SDS surfactant can have an enormous effect on the stability of suspension (i.e: zeta potential). *Li et al.* have reported that using ZnO nanoparticles with SDS surfactant has altered zeta potential from 17.56 ± 2.13 to −27.96 ± 2.59 mV. The results shown that increasing the surfactant concentration increase zeta potential towards the negative side.

References

1. Saidur, R.; Leong, K. Y.; Mohammad, H. A. A review on applications and challenges of nanofluids. *Renewable and Sustainable Energy Reviews* **2011**, 15, 1646–1668.
2. Alomair, O. A.; Matar, K. M.; Alsaeed, Y. H. Experimental Study of Enhanced-Heavy-Oil Recovery in Berea Sandstone Cores by Use of Nanofluids Applications. *Society of petroleum engineers* **2015**, 18.
3. Singh, P.; Bhat, S. Nanologging: Use of Nanorobots for Logging. SPE Eastern Regional Meeting **2006**.
4. Nikitin, A.; Korjik, M. An Impact of Nanotechnology on the Next Generation of Neutron Porosity LWD Tools. SPE International Oilfield Nanotechnology Conference and Exhibition **2012**.
5. Campos-Delgado, J.; Baptista, D. L.; Fuentes-Cabrera, M.; Sumpter, B. G.; Meunier, V.; Terrones, H.; Kim, Y. A.; Muramatsu, H.; Hayashi, T.; Endo, M.; et al. Nanodrilling: Iron Particle Nanodrilling of Few Layer Graphene at Low Electron Beam Accelerating Voltages (Part. Part. Syst. Charact. 1/2013). *Particle & Particle Systems Characterization* **2012**, 30, 75–75.
6. Kvítek, L.; Panáček, A.; Soukupová, J.; Kolář, M.; Večeřová, R.; Prucek, R.; Holecová, M.; Zbořil, R. Effect of Surfactants and Polymers on Stability and Antibacterial Activity of Silver Nanoparticles (NPs). *The Journal of Physical Chemistry C* **2008**, 112, 5825–5834.
7. Kelsall, R. W.; Hamley, I. W.; Geoghegan, M.; Kurzydłowski, K. J.; Ferenc, J. Nanotechnologie; Wydawnictwo Naukowe PWN: Warszawa, **2012**
8. Yu, W.; Xie, H. A Review on Nanofluids: Preparation, Stability Mechanisms, and Applications. *Journal of Nanomaterials* **2012**, 1–17.
9. Ayatollahi, S.; Zerafat, M. M. Nanotechnology-Assisted EOR Techniques: New Solutions to Old Challenges. SPE International Oilfield Nanotechnology Conference and Exhibition **2012**.

10. Ogolo, N.; Olafuyi, O.; Onyekonwu, M. Enhanced Oil Recovery Using Nanoparticles. SPE Saudi Arabia Section Technical Symposium and Exhibition **2012**.
11. Rezaei, A.; Abdi-Khangah, M.; Mohebbi, A.; Tatar, A.; Mohammadi, A. H. Using surface modified clay nanoparticles to improve rheological behavior of Hydrolized Polyacrylamid (HPAM) solution for enhanced oil recovery with polymer flooding. Journal of Molecular Liquids **2016**, 222, 1148–1156.
12. Salehi, M. M.; Hekmatzadeh, A.; Sajjadian, V. A.; Masoumi, M. Simulation of polymer flooding in one of the Iranian oil fields. *Egyptian Journal of Petroleum* **2017**, 26, 325–330
13. Cheraghian, G. Effect of nano titanium dioxide on heavy oil recovery during polymer flooding. *Petroleum Science and Technology* **2016**, 34, 633–641
14. Zargartalebi, M.; Barati, N.; Kharrat, R. Influences of hydrophilic and hydrophobic silica nanoparticles on anionic surfactant properties: Interfacial and adsorption behaviors. *Journal of Petroleum Science and Engineering* **2014**, 119, 36–43.
15. Li, S.; Hendraningrat, L.; Torsaeter, O. Improved Oil Recovery by Hydrophilic Silica Nanoparticles Suspension: 2-Phase Flow Experimental Studies. International Petroleum Technology Conference **2013**.
16. Mohajeri, M.; Hemmati, M.; Shekarabi, A. S. An experimental study on using a nanosurfactant in an EOR process of heavy oil in a fractured micromodel. *Journal of Petroleum Science and Engineering* **2015**, 126, 162–173.
17. Cheraghian, G. Effects of titanium dioxide nanoparticles on the efficiency of surfactant flooding of heavy oil in a glass micromodel. *Petroleum Science and Technology* **2016**, 34, 260–267.
18. Zaid, H. M.; Latiff, N. R. A.; Yahya, N. The Effect of Zinc Oxide and Aluminum Oxide Nanoparticles on Interfacial Tension and Viscosity of Nanofluids for Enhanced Oil Recovery. *Advanced Materials Research* **2014**, 1024, 56–59.

19. Fatehah, M. O.; Aziz, H. A.; Stoll, S. Stability of ZnO Nanoparticles in Solution. Influence of pH, Dissolution, Aggregation and Disaggregation Effects. *Journal of Colloid Science and Biotechnology* **2014**, 3, 75–84.
20. Mudunkotuwa, I. A.; Rupasinghe, T.; Wu, C.-M.; Grassian, V. H. Dissolution of ZnO Nanoparticles at Circumneutral pH: A Study of Size Effects in the Presence and Absence of Citric Acid. *Langmuir* **2012**, 28, 396–403.
21. Liu, W.-S.; Peng, Y.-H.; Shiung, C.-E.; Shih, Y.-H. The effect of cations on the aggregation of commercial ZnO nanoparticle suspension. *Journal of Nanoparticle Research* **2012**, 14.
22. Tang, F.; Uchikoshi, T.; Sakka, Y. Electrophoretic Deposition Behavior of Aqueous Nanosized Zinc Oxide Suspensions. *Journal of the American Ceramic Society* **2002**, 85, 2161–2165.
23. Sadowski, Z.; Polowczyk, I. Agglomerate flotation of fine oxide particles. *International Journal of Mineral Processing* **2004**, 74, 85–90.
24. Adil, M.; Zaid, H. M.; Chuan, L. K.; Latiff, N. R. A. Effect of Dispersion Stability on Electrorheology of Water-Based ZnO Nanofluids. *Energy & Fuels* **2016**, 30, 6169–6177.
25. Fiedot, M.; Rac, O.; Suchorska, P.; Karbownik, I.; Teterycz, H. Polymer – surfactant interactions and their influence on zinc oxide nanoparticles morphology. In Manufacturing Nanostructures; One Central Press (OCP): Cheshire, United Kingdom.
26. Li, X.; Yoneda, M.; Shimada, Y.; Matsui, Y. Effect of surfactants on the aggregation and sedimentation of zinc oxide nanomaterial in natural water matrices. *Science of The Total Environment* **2017**, 581-582, 649–656.

Chapter 4

Experimental Methods and Materials

4.1. Materials and supplies

The materials used in the experimental work can be divided into three phases similar to the experimental work itself.

1) Nanomaterials' synthesis and characterization.
2) Polymerization of polyacrylamide polymers (PAM).
3) Core flooding and its preliminary experiments.

Phase 1 – Nanomaterials' synthesis and characterization

Ethanol, Zinc acetate with purity of 99.99 % and Titanium foil of thickness 0.25 mm and purity 99.99 % were purchased from Merck. While Sodium hydroxide pellets were purchased from Alfa Aeser.

4.2. Synthesis

4.2.1. Titanium dioxide synthesis

The only structure synthesized in the case of Titanium dioxide was Nanotubes by breakdown anodization.

The titanium foil was ultrasonically cleaned with acetone, ethanol, and water respectively. The anodization technique for the electrochemical cell was set by a platinum foil as a counter electrode at the cathode while having the titanium at the anode with a size of 10 mm x 10 mm. A beaker was set in the middle of ice bath during the anodization process. Both electrodes were immersed in a beaker that was filled with 50 ml of 0.1M perchloric acid. The electrodes were connected to the power supply at 20 V starting gradually until the whole foil sample turns into powder. To ensure the good surface of the tubes; the obtained powder was washed several times with distilled water and centrifuged for 30 minutes.

The acquired powder after centrifugation was dried overnight in desiccator [1].

4.2.2. Zinc Oxide nanostructures synthesis

Since Zinc oxide can be easily shaped into many various structures [2], more structures were synthesized than that with the titanium dioxide case. Zinc oxide structures that have been successfully synthesized are nanoparticles, nanocubes, nanorods, nanoleaves, nanoflowers, and nanofibers.

4.2.2.1.Nanoparticles:

Zinc acetate and methanol were mixed by stirring for 10 minutes at room temperature then moved to vigorous stirring at a temperature of 80 ^{o}C. The obtained powder was annealed at 450 ^{0}C for 6 hours [3].

4.2.2.2.Nanocubes:

Zinc acetate and sodium hydroxide solutions were prepared then sodium hydroxide was added by dropwise to the zinc acetate solution forming a gel. The gel was initially filtrated using a filter paper then dried at 120 ^{0}C. After challenging trials, and huge changes in the morphology outcome every time; it has been discovered the optimized pH for a producible nanocube which is 9 [4, 5, and 6].

4.2.2.3.Nanorods Nanorods/ Nanoleaves/ Nanoflowers:

All the previous three structures were made using the same technique but by altering molar ratios. Zinc acetate and sodium hydroxide solutions were prepared and initially cooled down by an ice bath. Sodium hydroxide solution was added dropwise while stirring mechanically at high 550 rpm. The resulting solution was kept in water bath at a temperature of 70 ^{o}C for 30 minutes. The solution was filtered and the obtained powder was kept in a dust free environment overnight [7].

4.2.2.4.Nanofibers:

A weight of 1 g of zinc acetate was added to 2 g of PVP and dissolved in 10 ml of DMF. The powders are totally dissolved through vigorous stirring until no more polymer lumps are left in the solution under room temperature. The solution was loaded into 6 ml syringe and set in the electrospinner under optimization conditions. The resulting fibers were annealed at 500 °C for 4 hours in air, of 1 degree Celsius per minute of up and down rates [8].

Phase 2 – Polymerization:

4.3. Polymerization

Two polymers were used in the experimental work; Guar gum polymer, to evaluate the effect of ZnO on biopolymers, and polyacrylamide to assess the effect of ZnO on synthetic polymers.

4.3.1. Polyacrylamide polymerization

After challenging trials and errors through literature, polymerization has been executed through the following steps in order to ensure maximum growth of chains as well as an optimum environment for the initiator to work efficiently. Firstly, 50 g of acrylamide monomer was added to 400 ml of distilled water in a conical flask and stirred well until fully dissolved. Secondly, 0.1 g of acrylic acid was added and left for the same rpm of stirring at room conditions for 30 mins. Thirdly, 5 g of sodium acetate was added to the solution and left under stirring until the solution is clear. Finally, the whole flask was moved in a water bath of temperature 65 °C and 0.2 g of the initiator potassium persulfate was added to the solution. The resulting gel was dried in a Heratherm oven for 2 days until fully dry. In order to obtain the powder which will be used later in different concentrations; the resulting solid material was grinded. Finally, based on the calculations, the polymer of 2,000 ppm was prepared as blank and mixed with nanoparticles for rheology tests [9].

4.3.2. Guar gum

Guar Gum was purchased as ready-made polymer from Merck. Three different concentrations

(0.5%, 1 %, 3%) of each the selected ZnO nanostructure (nanoparticles, nanocubes, and nanofibers) were well dispersed in 100 ml of distilled water by homogenizer at 1750 rpm. After total dispersion, the polymer was added to the suspension and stirred well for 10 mins.

4.4. Characterization:

The previously mentioned nanostructures were all characterized by Scanning Electron Microscopy (SEM), Energy-dispersive X-ray spectroscopy (EDX), X-Ray Diffraction (XRD), and Brunauer–Emmett–Teller (BET) as preliminary basic tests. Based on the results of the previously mentioned characterization techniques; specific zinc oxide nanostructures; (nanoparticles, nanocubes, and nanofibers), were selected to be used for further tests. The zinc oxide variety of structures made it more ideal to show the effect of morphology on the polymer's stability during the core flooding process.

4.4.1. Water uptake for Polyacrylamide

Samples were weighed prior to water and then immersed in water for different times. After removal the samples were wiped with tissue paper to remove excess water on the surface and then reweighed, the process was repeated after regular time intervals to find out the amount of water absorbed as a function of time. Water absorption capacity (ω) was determined from the relationship.

$$(\omega)\% = \frac{\omega - \omega_0}{\omega} \times 100$$

where W_0 and W are the weights of the polymer samples before and after immersion in water respectively.

4.4.7. Rheology tests for polyacrylamide

The rheology tests were very crucial before starting the core flood because it will define the parameters for the final phase which is core flooding. The basic rheology measurements taken were viscosity at different shear rates, different temperatures, and different salinities. The rheology tests also give an insight of how much the polymer has improved/deteriorated using the ZnO nanomaterial.

4.4.8. Thermogravimetric analysis (TGA) test for Guar Gum

Three different concentrations (0.5%, 1 %, 3%) of selected ZnO nanostructure (nanocubes, nanoparticles, and nanofibers) were well dispersed in 100 ml of distilled water by homogenizer at 1750 rpm. After total dispersion, the polymer was added to the suspension and stirred well for 10 mins. The prepared nanocomposites were dried at 60 °C in an oven overnight until they are fully dry and turned into thin films. The thin films were investigated by TGA for thermal stability in comparison with the pure polymer as a control.

Phase 3 – Core flooding:

Prior to core flooding, it was essential to make other measurements required to ensure the effectiveness of the nanoparticles fluid in porous media as well as their stability.

4.4. Nanofluids prelimenary tests

Zinc oxide nanofluids are prepared at different concentrations (0.05, 0.1, 0.2, and 0.3) weight percent. Initially using deionized water (DIW) at normal pH (7.7). However, after mixing for 10 minutes and sonication for 10 minutes; the particles did not suspend. Thus, the pH of the solution was increased to 12 using NaOH based on the work of *Fatehah et al.* in 2014 and others that investigated the zeta potential behavior of different pHs of zinc oxide nanofluids [19 - 21]. The zinc oxide nanostructures were successfully suspended in DIW after sonication for 10 minutes. Using visual observation the suspensions precipitated only after 6 hours. Many reviews have asserted that polymers and surfactants could be used to stabilize zinc oxide nanofluids. Hence, as a first attempt, two batches of polyacrylamide (PAM) polymer of concentration 2,000 ppm were mixed with the nanostructures at the previously mentioned concentrations for 10 minutes by ultrasonication at pH 8.5 as well as pH 12. Although the suspensions were stable for almost 36 hours through visual observations; it was observed that the 0.3 weight percent was the first to precipitate in both water and polymer solutions. Looking for longer stability time, it has

been decided to use a surfactant in order to suspend ZnO nanostructures for a longer time. Different reviews were using different surfactants; thus CTAB (Cetyltrimethylammonium bromide) as well as SDS (Sodium dodecyl sulfate) and SDBS (Sodium dodecyl benzene sulfonate) [22, 23]. The surfactants were used either by based on CMC (critical micelle concentration) only or both CMC and other concentrations. The concentrations selected for the previously mentioned surfactants were based on previous relevant literature review. A stock for each of the surfactants used was prepared; then smaller concentrations where prepared off the stock using dilution method using the dilution equation below:

$$C_1V_1 = C_2V_2 \qquad \text{[Equation 4.1]}$$

Since surfactants augmented nanoparticles nanofluid suspensions showed the best stability compared to DIW or PAM; the suspensions stability was monitored visually as well as using a spectrophotometer. Another important reason is to make use of interfacial tension further reduction by using zinc oxide nanoparticles rather than using more surfactant.

In order to efficiently evaluate the parameter being investigated; each experiment should have only one variable at a time. Changing too many parameters would give faulty observations about the changing parameters and may end up in the wrong conclusion. Thus, preliminary tests were divided into the following minor experiments. Firstly, (water, ZnO NPs-percentage, pH) was prepared by mixing the tabulated quantities of nanoparticles in **(Table 4-1)** for 10 minutes followed by sonication for 10 minutes. As shown in **(Figure 4-1)**, visual observation was taken for each sample prepared after its preparation as well as after 24 hours.

Table 4 - 1: 1st preliminary test.

No.	Label	Fluids	Nano-conc.	Quantities (g)
1	W	Water, n-dodecane	0	0
2	W, 0.05 NP, PH12	Water, n-dodecane	0.05 wt %	0.01
3	W, 0.1 NP, PH12	Water, n-dodecane	0.1 wt %	0.2
4	W, 0.2 NP, PH12	Water, n-dodecane	0.2wt %	0.04
5	W, 0.3 NP, PH12	Water, n-dodecane	0.3 wt %	0.06

Figure 4 - 1: DIW+ various nanoparticles percentage at preparation time (zero hour).

Secondly, using the same conditions and the same nano-concentrations, the stability of ZnO NPs suspensions in PAM polymer was assessed. The details of the experiment is shown below in **(Table 4-2)**. The same time was used for mixing and sonication as in the 1st preliminary test.

Figure 4 - 2: Polyacrylamide + ZnO nano-suspensions at different concentration at preparation time (zero hour).

Table 4 - 2: 2nd preliminary test.

No.	Label	Fluids	Nano-conc.	Quantities (g)
1	PAM, pH 12	PAM, n-dodecane	0	0
2	PAM, 0.05 NP, pH12	PAM, n-dodecane	0.05 wt %	0.01
3	PAM, 0.1 NP, pH12	PAM, n-dodecane	0.1 wt %	0.2
4	PAM, 0.2 NP, pH12	PAM, n-dodecane	0.2wt %	0.04
5	PAM, 0.3 NP, pH12	PAM, n-dodecane	0.3 wt %	0.06

After visual results showing that PAM + nano suspensions were more stable than DIW + nano suspensions. It was essential to characterize stability by some sort of physical meaning using UV spectrophotometer under absorption wavelength was set to 440 nm. Each of the first two preliminary tests were evaluated by tensiometer to ensure any effect of IFT reduction. Thirdly, it was essential to investigate the effect of different surfactants (SDS, SDBS, CTAB) when added to various nanoparticles percentages on both stability and IFT. Since it was observed the fast precipitation of 0.3% nanoparticles. Thus, the highest percentage of nanoparticles used was 0.2 wt %. **(Table 4-3 and 4-4)** show the details of the experiment regarding concentrations of both the surfactant as well as the nanoparticles.

Table 4 - 3: 3rd preliminary test for anionic surfactants.

No.	Label	Fluids	Nano-conc.	Quantities (g)
1	0.025 SDBS	0.025 wt % SDBS, n-dodecane	0	0
2	0.025 SDBS, 0.05 NP, pH7.7	0.025 wt % SDBS, n-dodecane	0.05 wt %	0.01
3	0.025 SDBS, 0.1 NP, pH7.7	0.025 wt % SDBS, n-dodecane	0.1 wt %	0.2
4	0.025 SDBS, 0.2 NP, pH7.7	0.025 wt % SDBS, n-dodecane	0.2 wt %	0.4
5	0.017 SDBS	0.017 wt % SDBS, n-dodecane	0	0
6	0.017 SDBS, 0.05 NP, pH7.7	0.017 wt % SDBS, n-dodecane	0.05 wt %	0.01
7	0.017 SDBS, 0.1 NP, pH7.7	0.017 wt % SDBS, n-dodecane	0.1 wt %	0.2
8	0.017 SDBS, 0.2 NP, pH7.7	0.017 wt % SDBS, n-dodecane	0.2 wt %	0.4

Table 4 - 4: 3rd preliminary test for cationic surfactants.

No.	Label	Fluids	Nano-conc.	Quantities (g)
1	0.025 SDBS at pH 12	0.025 wt % SDBS, n-dodecane	0	0
2	0.025 SDBS, 0.05 NP, pH 12	0.025 wt % SDBS, n-dodecane	0.05 wt %	0.01
3	0.025 SDBS, 0.1 NP, pH 12	0.025 wt % SDBS, n-dodecane	0.1 wt %	0.2
4	0.025 SDBS, 0.2 NP, pH 12	0.025 wt % SDBS, n-dodecane	0.2 wt %	0.4
5	0.0146 CTAB at pH 7.7	0.0146 wt % CTAB, n-dodecane	0	0
6	0.0146 CTAB, 0.05 NP, pH 7.7	0.0146 wt % CTAB, n-dodecane	0.05 wt %	0.01
7	0.0146 CTAB, 0.1 NP, pH 7.7	0.0146 wt % CTAB, n-dodecane	0.1 wt %	0.2
8	0.0146 CTAB, 0.2 NP, pH 7.7	0.0146 wt % CTAB, n-dodecane	0.2 wt %	0.4

SDS surfactant was investigated at selected points of constant concentration of 0.2 weight percent (CMC) and three concentrations of nanoparticles including 0.05, 0.1, and 0.2 weight. The main objective of the previously mentioned experiments is to find the most stable suspension conditions as well as possible effects on IFT to help later on through oil recovery during core flood tests.

4.5. Interfacial tension (IFT) measurements

The interfacial tension was measured using a tensiometer K9 (Kruss) shown in **(Figure 4-3)** through Du Nouy ring method. The tensiometer works through making use of the force used to pull the ring off the fluids interface. The ring is made of platinum – iridium which allows the tensiometer to sense a wettability of contact angle of zero degree. The tensiometer can record the maximum mechanical force required to detach the ring from the fluid interface. Afterwards, the tensiometer applied the equation below to calculate and display the interfacial tension:

Figure 4 - 3: K9 (Kruss) Tensiometer. (Teesside University, 2017)

$$\sigma = \frac{F}{4\,\mu\,R} \qquad \text{[Equation 4.2]}$$

where σ is the interfacial tension, F is the mechanical force required to pull the ring off the fluid, and R is the radius of the ring. The schematic shown in **(Figure 4-4)** gives an idea about the concept of how the tensiometer works through the interaction between the ring and the fluid.

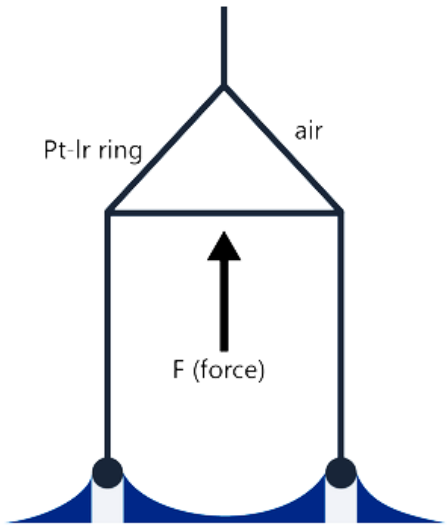

Figure 4 - 4: Tensiometer concept.

4.6. Stability:

The stability measurements were measured using ultraviolet- visible spectrophotometer (JENWAY 7300) shown in **(Figure 4-5)**.

Figure 4 - 5: Spectrophotometer JENWAY 7300.

The measurement mechanism is based on Beer-Lambert Law which mainly states that the amount of light absorbed by a medium is independent on the light's intensity. However, it depends on the concentration of the absorbing medium as well as its thickness. The law can be expressed by the equation below:

$$A = \log\frac{I_0}{I} = \log\frac{100}{T} \qquad \text{[Equation 4.3]}$$

where A stands for the absorbance, I_0 is the intensity of the incident light, I is the intensity of transmitted light, and T is the transmittance. The main parts of the spectrophotometer are shown in **(Figure 4-6)**. The source emits light that goes to monochromator where it gets isolated of a single wavelength. Afterwards, it gets to the sample compartment where it gets absorbed/transmitted. The transmitted light then passes on to the detector where absorbance gets measured and displayed on the readout screen.

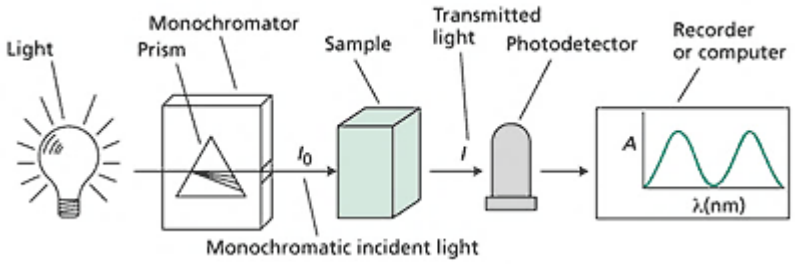

Figure 4 - 6: The main parts of the spectrophotometer [25].

The absorbance of each of the samples mentioned in the previous section was plotted versus time to figure out the most stable sample by comparing their slope.

4.7. Core flooding

The core flooding phase was performed in Teesside University's laboratory for petroleum engineering using the following materials and devices.

4.7.8. Core samples

The rock samples used were at first were limestone but through the progress of measurements and knowledge about the new events happening during research, limestone samples were not used. Instead, sandstone core samples of dimensions (D = 2.52 cm, L = 6.72 cm). Laboratory measurements through core flooding and mathematical measurements showed that the core samples had porosity around 26.51 % and absolute permeability of 28.137 md. The core samples were characterized morphologically and elementally using SEM and EDX to acquire more data about the mineralogy of the core samples.

- **Core samples cleaning**

The core samples were cleaned using VINCI Soxhlet Extractor which cleans core samples from original fluids or any other materials.

The core samples that are aimed to be cleaned are soaked in alcohol in the sample chamber. The

solvent gets heated until vapors travel to the top of the sample chamber where it meets up with a cold trap. Vapors get condensed and get back again in the sample chamber. The contaminated solvent is extracted out of the sample chamber by siphon and returned to the flask where it will be redistilled. The extraction process was performed in 48 hours to ensure the removal of all contaminants originally in the core sample.

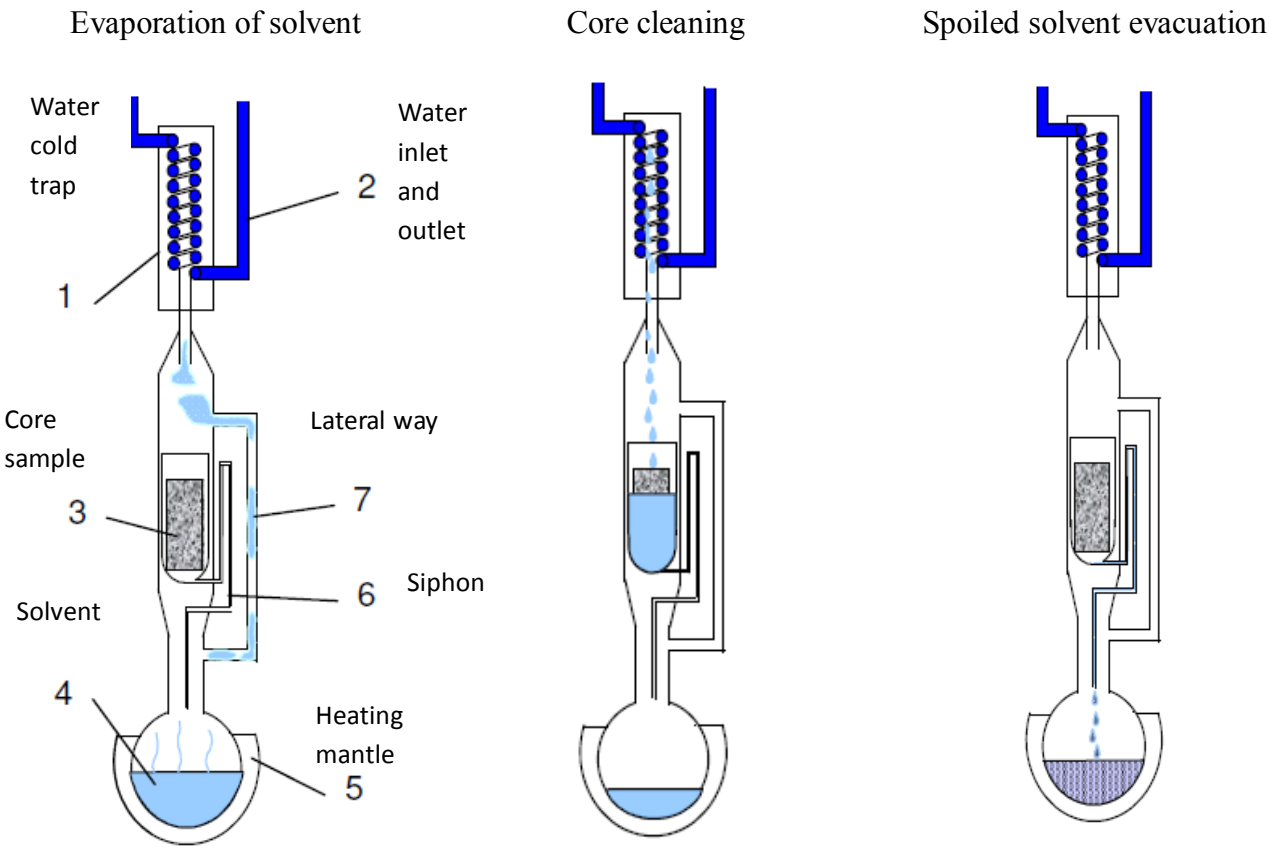

Figure 4 - 7: Soxhlet extractor schematic. (VINCI Soxhlet extractor manual).

- **Porosity measurement**

Using the widely known equation shown below that relates to mass, weight, and density; the pore volume could be calculated or simply using the volume of a cylinder equation. The pore volume can be used later to calculate effective porosity.

$$\text{Pore volume (V)} = \frac{m_{\text{saturated sample}} - m_{\text{dry sample}}}{(\rho)_{\text{saturation fluid}}} \qquad \text{[Equation 4.4]}$$

To make use of the previously mentioned equation; a vacuum saturator shown in **(Figure 4-8)** was used to saturate the core samples. The saturation process can be presented in three main stages. Firstly, the vacuum pump is used at pressure 10 bar for 3 hours to evacuate any air pockets inside the sample. Secondly, the core samples were allowed to saturate by disconnecting the vacuum hose and disconnecting the pump; then filling the evacuated chamber at atmospheric pressure with the saturation liquid. Finally, the hand pump is used to pressurize the saturation liquid surrounding the cores to 2,000 psi overnight. After releasing the pressure on the pump back to atmospheric and removing the samples; their weight after saturation was used with the above equation to calculate the pore volume and hence calculate porosity using the equation below:

$$\text{Porosity } (\emptyset) = \frac{\text{Pore volume } (V_p)}{\text{Bulk volume } (V_B)} \qquad \text{[Equation 4.5]}$$

Figure 4 - 8: Vacuum saturator (Teesside University, 2017).

- **Permeability measurements**

The absolute permeability has been measured using Benchtop Relative Permeameter System, BRP 350. The schematic in **(Figure 4-9)** shows the components of the core flood setup. Initially, the core sample was placed in the core holder and a confining pressure of 2,500 psi was applied to the core to avoid injection fluids from flowing around the core. Firstly, the core was injected by DIW to ensure the sample's full saturation using BRP 350 single piston pump and to calculate the absolute permeability. The used pump allows for constant flow over a wide pressure range during the procedure. Using Darcy law **(Equation 4.6)** permeability was calculated assuming a DIW viscosity of 1.02 cp.

$$\frac{q}{A} = \frac{K\,(P_1 - P_2)}{\mu * L} \qquad \text{[Equation 4.6]}$$

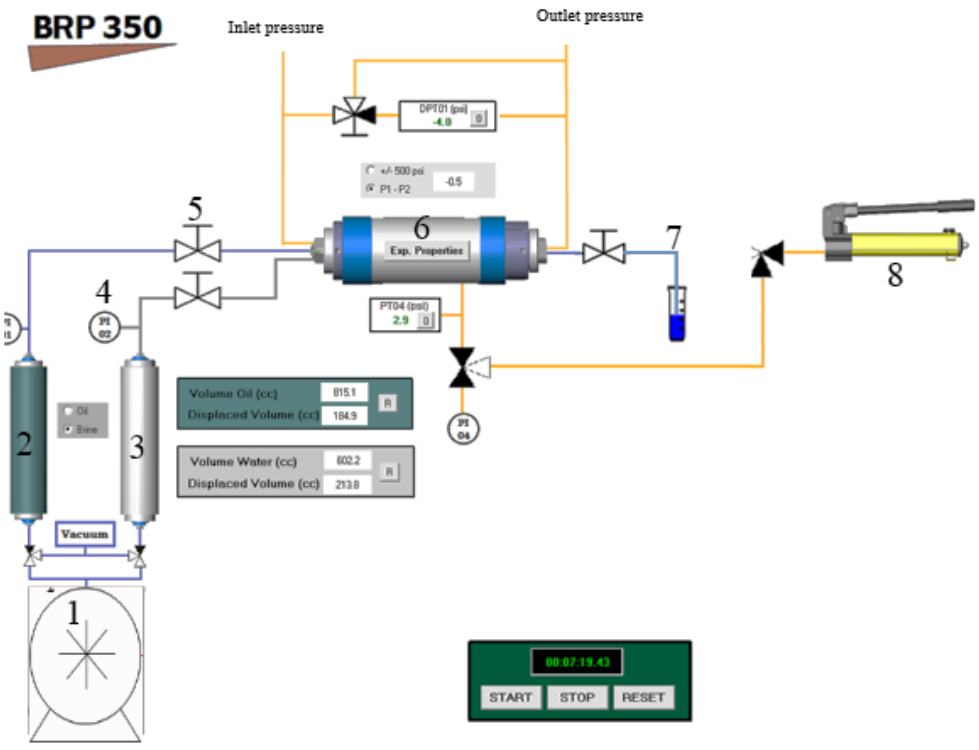

Figure 4 - 9: Schematic for BRP 350 core flood setup.

The software uses linear regression technique to calculate the average permeability (K) using Darcy law. It uses 3 different flow rates (q), cross-sectional area (A), fluid viscosity (μ), core length (L),

and ($P_1 - P_2$) as the pressure drop across the core sample.

4.7.9. Nanomaterials

Zinc oxide suspensions were only used at this stage based on the previously executed tests and their results. Based on literature, it was hypothesized that ZnO suspension in SDS flooding would show better results in oil recovery due to expected interfacial tension reduction.

- **Nanofluid preparation for core flood**

A mixture of 0.2 weight percent SDS and the 0.05 weight percent of ZnO nanoparticles were mixed through sonication for 15 minutes while using water bath to avoid undesired heating.

4.7.10. N-dodecane:

A colorless liquid that is less dense than water and insoluble in it commonly used to substitute for the usage of crude oil in experimental work.

- **Core flooding setup**

The main target of the whole previously mentioned work was to investigate the effect of different morphologies of zinc oxide on the performance of surfactant polymer flooding in oil recovery. However, it has been discovered from rheology the negative influence of zinc oxide on polyacrylamide. Subsequently, it has been decided to use zinc oxide nanoparticles suspensions in SDS surfactant flooding in comparison with conventional SDS surfactant flooding. It has been widely known that a core flood setup is the best tool that can show the previously mentioned required aim. The core flood setup used in the experiment is Benchtop Relative Permeameter System, BRP 350 shown in **(Figure 4-10)**. The relative permeameter is composed of two accumulators for displacing fluids (DIW/nanofluid, n-dodecane). In addition, it consists of a single piston pump to inject one fluid at a time into the vessels to reach the core holder. In order to avoid fluid flow around the core sample, a confining pressure of 2,500

psi was applied. The experiments were executed in conditions of ambient temperature, 2500 psi pressure, and different flow rates.

Initially, water saturation was 100% in the core samples from the previous step. Absolute permeability measurement started by injecting DIW by flow rates (2.0 ml/min, 3.0 ml/min, 4.0 ml/min) until the pressure reached stability phase. Afterwards, the oil injection was applied in two flow rates (0.5 ml/min, and 1 ml/min) until reaching the connate water saturation. (i.e.: no more water produced from the core).

For water flooding, DIW was injected in the core samples until reaching the residual oil saturation. Finally, in order to conclude the experiment, tertiary recovery was performed once by SDS surfactant and another time by injecting (zinc oxide nanoparticles + SDS). Additional oil produced through nanofluid injection would prove the potential use of zinc oxide nanofluid. Through the preliminary previous tests as well as core flood experiments it is possible to report whether the difference in morphology has any effect on the oil recovery. There are series of equations used to calculate the recovery factor from the results of the above procedures:

Figure 4 - 10: Core flood setup (Teesside University, 2017)

A: dead volume + pore volume.

B: Volume of DIW displaced by oil.

C: Volume of DIW remained in the core = A – B

Initial water saturation, $S_{wi} = \frac{C}{Pore\ volume}$

Initial oil saturation, $S_{oi} = 1 - S_{wi}$

E = Initial oil in place (IOIP) = pore volume * S_{oi}

D: volume of oil produced after DIW injection.

Recovery factor (R.F) = $\frac{D}{E}$

F: volume of oil produced after nanofluid displacement.

Residual oil saturation after nanofluid $S_{orn} = \frac{B-D-E-F}{B}$

Recovery factor due to nanofluid displacement, $RF_n = \frac{1-Swi-Sorn}{1-Swi}$

References:

1) Antony, R. P.; Mathews, T.; Dasgupta, A.; Dash, S.; Tyagi, A.; Raj, B. Rapid breakdown anodization technique for the synthesis of high aspect ratio and high surface area anatase TiO2 nanotube powders. *Journal of Solid State Chemistry* **2011**, 184, 624–632.
2) Wang, Z. L. Zinc oxide nanostructures: growth, properties and applications. *Journal of Physics: Condensed Matter* **2004**, 16, R829–R858.
3) Sayari, A.; Mir, L. E. Structural and Optical Characterization of Ni and Al Co-Doped ZnO Nanopowders Synthesized via the Sol-Gel Process. *KONA Powder and Particle Journal* **2015**, 32, 154–162.
4) Alias, S. S.; Mohamad, A. A. Synthesis of Zinc Oxide by Sol–Gel Method for Photoelectrochemical Cells. *Springer Briefs in Materials* **2014**.
5) Alias, S.S., Ismail, A.B., Mohamad, A.A.: Effect of pH on ZnO nanoparticle properties synthesized by sol–gel centrifugation. *J. Alloy. Compd*. 499, 231–237 (**2010**)
6) Rani, S., Suri, P., Shishodia, P.K., Mehra, R.M.: Synthesis of nanocrystalline ZnO powder via sol–gel route for dye-sensitized solar cells. *Sol. Energy Mater. Sol. Cells* 92, 1639–1645 (**2008**)
7) Kumar, K. M.; Mandal, B. K.; Naidu, E. A.; Sinha, M.; Kumar, K. S.; Reddy, P. S. Synthesis and characterisation of flower shaped Zinc Oxide nanostructures and its antimicrobial activity. *Spectrochimica Acta Part A: Molecular and Biomolecular Spectroscopy* **2013**, 104, 171–174.
8) Zhu, Z.; Zhang, L.; Howe, J. Y.; Liao, Y.; Speidel, J. T.; Smith, S.; Fong, H. Aligned electrospun ZnO nanofibers for simple and sensitive ultraviolet nanosensors. *Chemical Communications* **2009**, 2568.

9) Feng, Q.; Lu, G.-D.; Liu, Y.-Q.; Yan, Q.-Z.; Ge, C.-C. Frontal Polymerization Of Acrylamide For Preparing Porous Polyacrylamide Hydrogel——Effects Of Initiator And Solvent On Propagation And Products. *Acta Polymerica Sinica* **2009**, 009, 674–679.

10) Allam, N. K. Techniques for structural characterization II. Advanced characterization techniques.

11) Joshi, M.; bhattacharyya, A.; Ali, S. W. Characterization techniques for nanotechnology applications in textiles. *Indian journal of fiber & textile research* **2008**, 33, 304–317.

12) Antolasic, F. RMIT School of Applied Sciences http://minyos.its.rmit.edu.au/~rcmfa/FTIR/asap2000/.

13) X- ray Diffraction (XRD) http://ywcmatsci.yale.edu/xrd (accessed Sep 9, **2017**).

14) Suryanarayaba, C.; Norton, M. G. X-Ray Diffraction A Practical Approach; *Springer Verlag*, **2014**.

15) X-ray Photoelectron Spectroscopy (XPS) http://ywcmatsci.yale.edu/xps.

16) Allam, N. K. Elemental Detection Techniques. X-ray photoelectron spectroscopy (XPS)

17) Mamdouh, W. M. Infrared spectroscopy. FTIR.

18) Analytical Spectroscopy by R.P.W. Scott http://www.analyticalspectroscopy.net/ (accessed September 9, **2017**).

19) Fatehah, M. O.; Aziz, H. A.; Stoll, S. Stability of ZnO Nanoparticles in Solution. Influence of pH, Dissolution, Aggregation and Disaggregation Effects. *Journal of Colloid Science and Biotechnology* **2014**, 3, 75–84.

20) Yu, W.; Xie, H. A Review on Nanofluids: Preparation, Stability Mechanisms, and Applications. *Journal of Nanomaterials*, **2012**, 1–17.

21) Tang, E.; Cheng, G.; Ma, X.; Pang, X.; Zhao, Q. Surface modification of zinc oxide nanoparticle by PMAA and its dispersion in aqueous system. *Applied Surface Science* **2006**, 252, 5227–5232.

22) Sadowski, Z.; Polowczyk, I. Agglomerate flotation of fine oxide particles. *International Journal of Mineral Processing* **2004**, 74, 85–90.

23) Adil, M.; Zaid, H. M.; Chuan, L. K.; Latiff, N. R. A. Effect of Dispersion Stability on Electrorheology of Water-Based ZnO Nanofluids. *Energy & Fuels* **2016**, 30, 6169–6177.

24) kruss-scientific https://www.kruss-scientific.com/services/education-theory/glossary/du-nouey-ring-method/

25) Plant Physiology and development, Sixth Edition http://6e.plantphys.net/topic07.01.html

5. Chapter 5

Results and Discussion

In this chapter, all results would be reported including those were not used in the final application. The main idea of scanning the synthesized samples by SEM to check the morphology of the synthesized samples and ensure it is in agreement with literature.

5.1. Morphological and structural characterization

5.1.1. Titanium dioxide nanotubes

The results in **(Figure 5-1)** shows a side view of the synthesized particles; the figure shows a stair-like structure of the synthesized nanotubes.

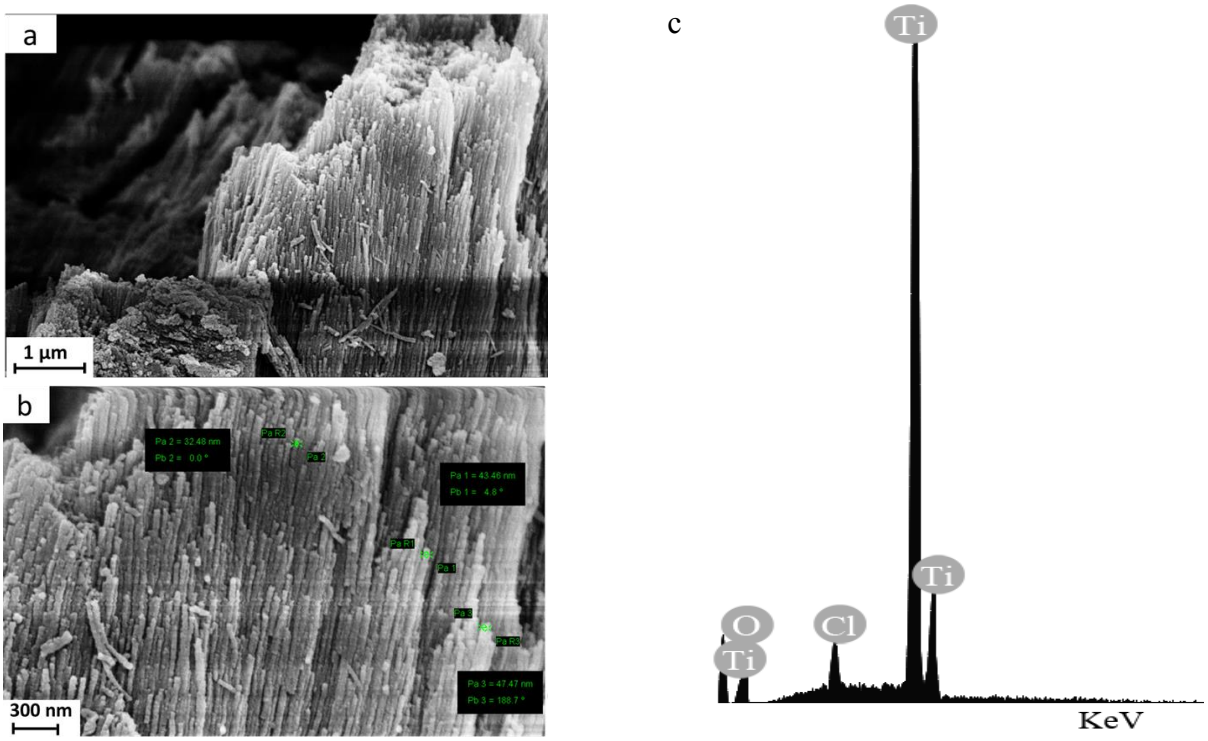

Figure 5 - 1: Titanium dioxide nanotubes structure and morphology through SEM and EDX.

The results show a uniform etching of the perchloric acid to the titanium foil used and hence showing single-walled nanotubes of outer diameter between 32 nm – 47 nm. By comparing the

synthesized nanotubes' diameter to previous studies; it is larger than some studies [1, 2] but within the range or others [3]. The length measured for the nanotubes bundles ranger between 7 µm – 16 µm.

5.1.2. Zinc oxide nanostructures:

5.1.2.1. Nanoparticles

After challenging trials and errors; it was possible to uniform spherical ZnO nanoparticles as shown in **(Figure 5-2)** that ranges in the particle size between 30 nm – 75 nm.

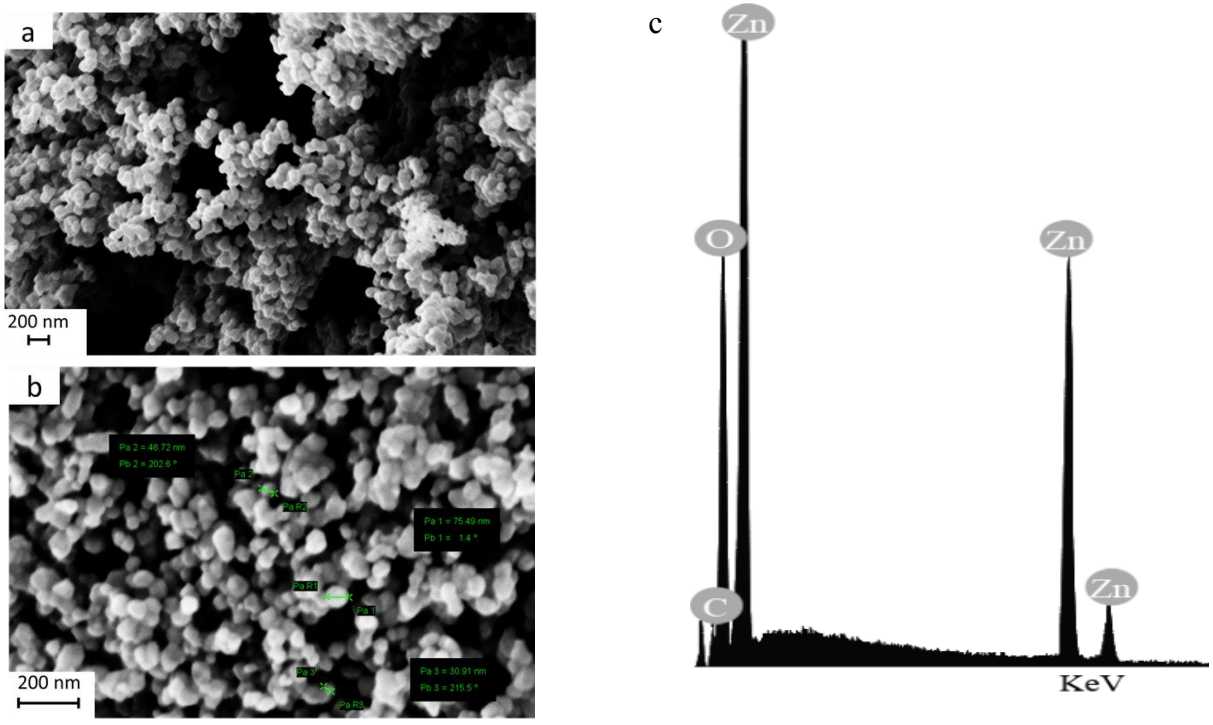

Figure 5 - 2: Zinc Oxide nanoparticles structure and morphology through SEM and EDX.

5.1.2.2. Nanocubes

After optimizing through different pH values; it was possible to synthesize uniform ZnO nanocubes that range in the particle size between 31 nm – 91 nm. As shown in **(Figure 5-3)**, the nanocubes are well optimized showing uniformity and homogeneity. In addition, the edges of the ZnO nanocubes are sharp compared to other nanocubes studies reported in previous studies which may account for the higher strain. Furthermore, the EDX analysis shows the presence of zinc and oxygen

only with no trace for any of the other reactants.

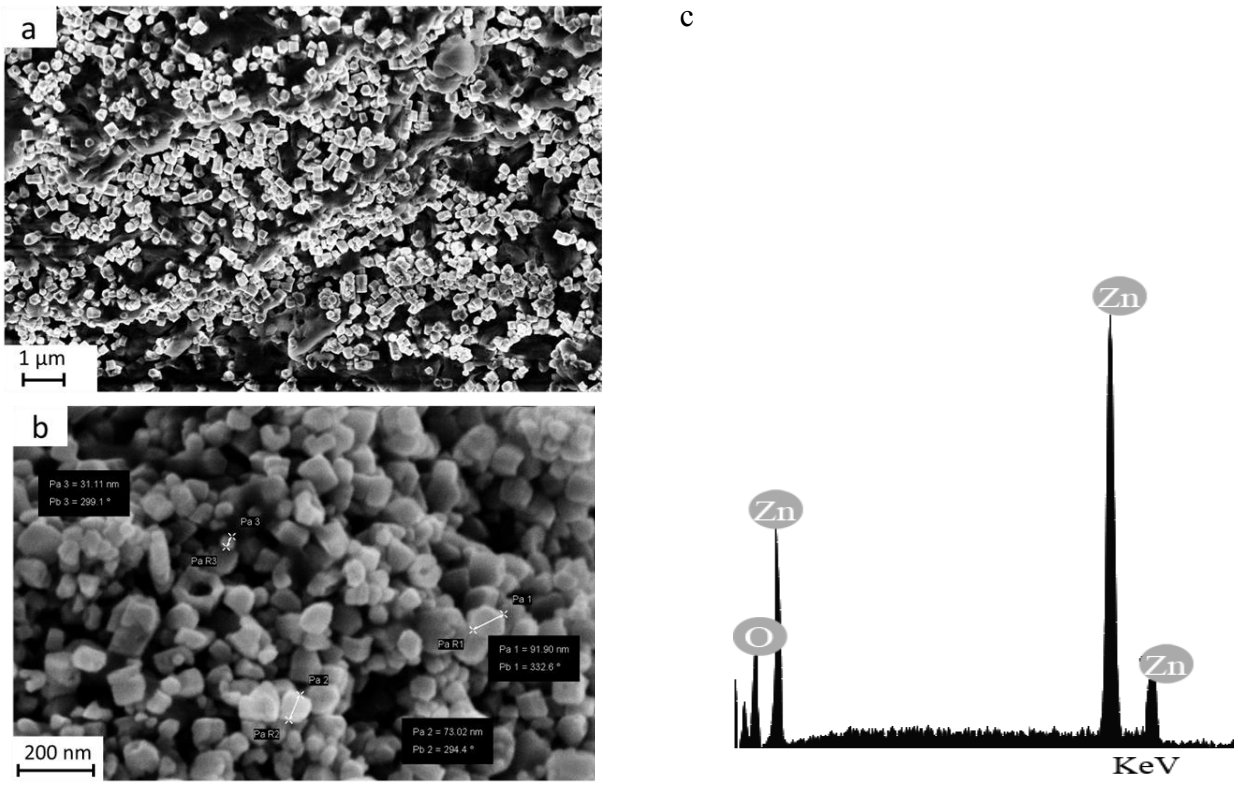

Figure 5 - 3: Zinc Oxide nanocubes structure and morphology through SEM and EDX.

5.1.2.3. Nanorods/ Nanoleaves/ Nanoflowers:

The nanorods, nanoleaves, and nanoflowers were not a part of the initial main plan made for that work. However, the synthesis technique was inspired by a hypothesized growth mechanism that was proposed by Kumar et al in 2013. It was possible to produce the mentioned nanostructures using the same technique but only by altering molar ratios of reactants as mentioned in chapter 4. As shown in **(Figure 5-4)**, the development of the nanostructures from one morphology to the next one is clear. Due to the limited time and the lack of intention to use those structures in the final application; the non-optimized conditions caused 2 structures to appear in the same sample SEM image sometimes.

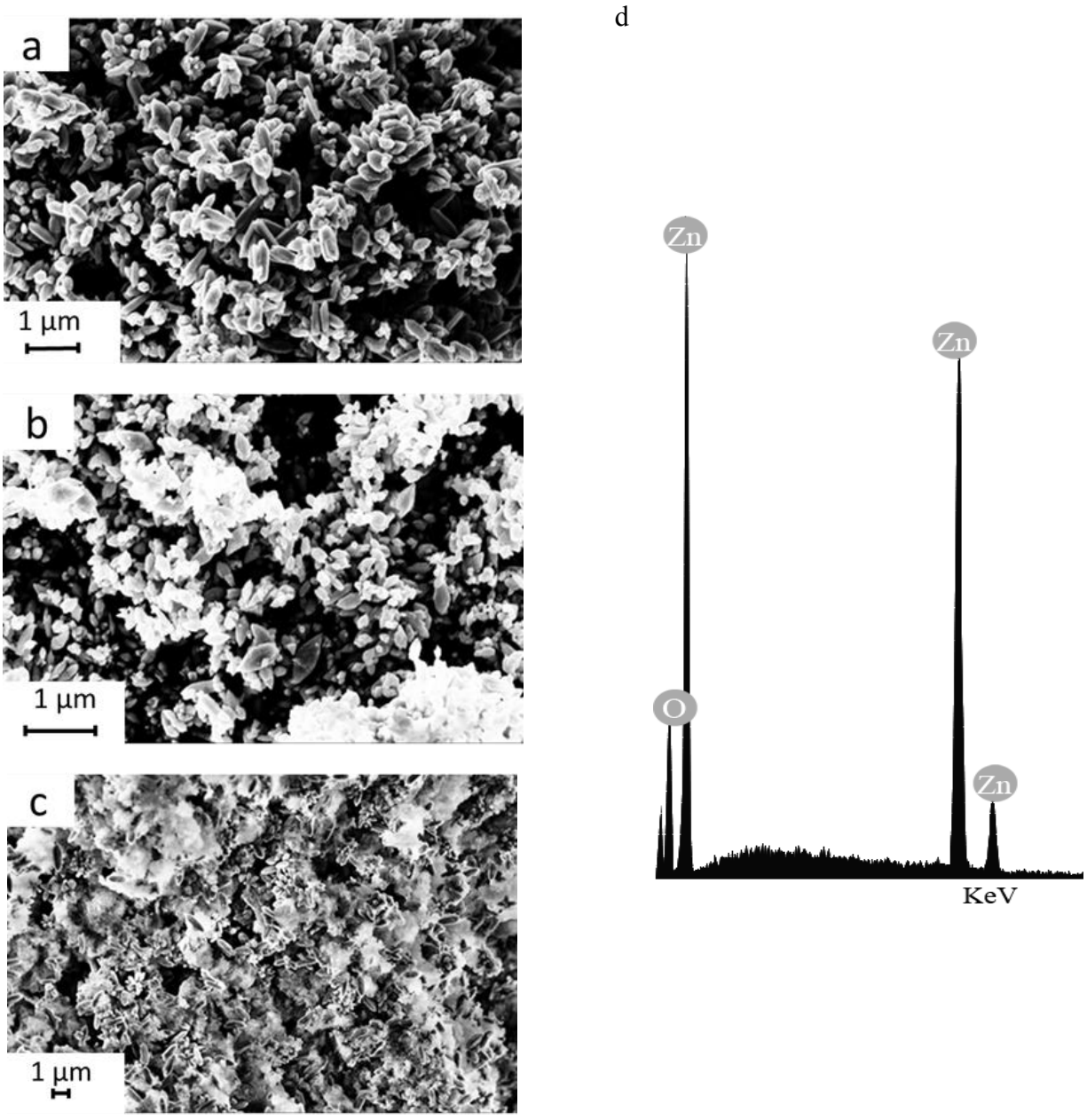

Figure 5 - 4: Zinc Oxide nanorods, nanoleaves, and nanoflowers structure and morphology through SEM and EDX.

5.1.2.4. Nanofibers:

The non-annealed nanofibers morphological testing as shown in **(Figure 5-5 a,b)**, show extremely uniform aligned zinc oxide nanofiber. To ensure the homogeneity, highly magnified images were taken to show that the fibers are not sticking together and that they are very smooth.

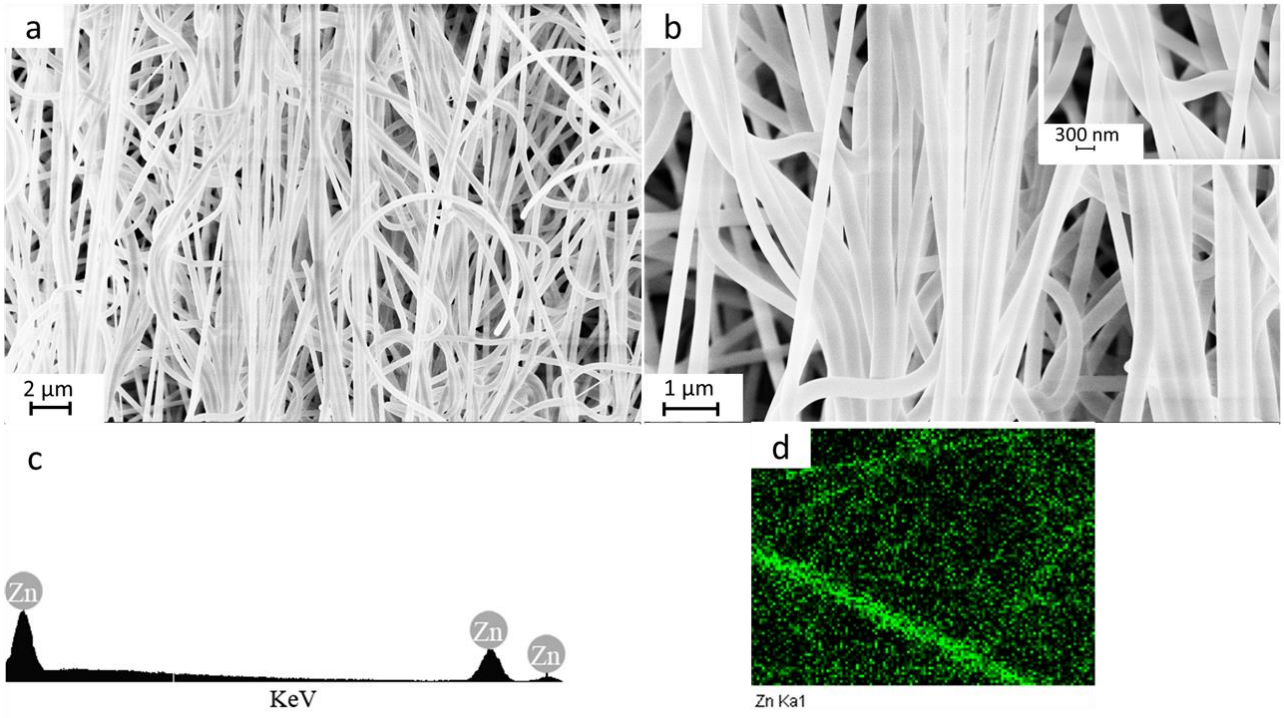

Figure 5 - 5: Non-annealed Zinc Oxide nanofibers structure and morphology through SEM and EDX.

It has been measured by SEM imaging that the diameter of the fiber is ranging between 210 - 235 nm. It was crucial to make sure before annealing the good distribution of Zinc throughout the length of the fiber. Thus, as shown in **(Figure 5-5 c,d)** ordinary EDX was performed to ensure the presence of zinc that was even confirmed for good distribution by EDX mapping. However, it can be shown in **(Figure 5-6)** the effect of the annealing conditions used. On one hand, it can be shown with **(Figure 5-6 a,b)** that under slow up and down rates it is possible for the fiber to keep its morphology. The fibers were made up of small zinc oxide nanoparticles after the evaporation of the PVP polymer. On the other hand, as shown in **(Figure 5-6 c,d)**, using a faster up rate and the same down rate as the previous condition caused the growth of nanoparticles into nanorods that coalesced into spherical shapes. The rods preferentially aligned themselves into a spherical shape having less surface area of the same volume. That can help the structure being less reactive by reducing the dangling bonds in it.

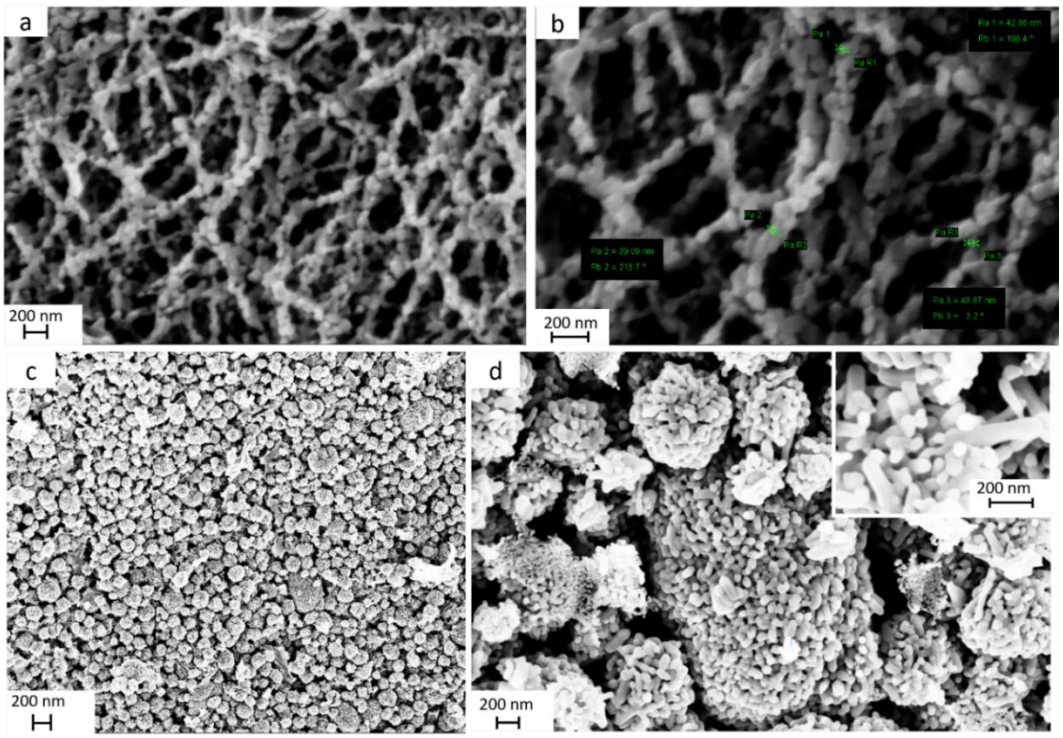

Figure 5 - 6: Annealed Zinc Oxide nanofibers a, b at annealing condition 1 while c, and d at condition 2

5.2. BET (Specific surface area measurements)

It was very important for any work to have a hypothesis for any work and to know what to expect as an outcome. Thus, the hypothesis was that the nanoparticles with the higher specific surface area should have more interaction with the other fluids in porous media and hence increase reactivity. All the synthesized nanostructures are tabulated in **(Table 5-1)** showing in descending order.

Table 5 - 1: BET measurements for different structures.

Zinc oxide structures	Specific surface area (g/m^2)	Titanium dioxide structures	Specific surface area (g/m^2)
Nanoparticles	13.5	Nanotubes	83.5
Nanocubes	7.5	Nanoparticles (P25)	48.1
Nanorods	6.5		
Nanoleaves	6.2		
Nanoflowers	6.4		
Nanofibers	4.2		

Although BET results show that TiO_2 has the higher specific surface area, zinc oxide was used for further testing instead of it. The variety of structures were possible to synthesize of zinc oxide made it a better candidate for further tests because it would be possible to investigate the effect of different morphologies. Subsequently, from BET results, zinc oxide nanoparticles, as well as nanocubes, were selected to use for the next tests.

5.3. XRD analysis:

XRD data analysis can help to find very useful and interesting data about the structures. The key of making a good use of the XRD data resides in making a good use of Bragg's law as well Scherrer equation. The zinc oxide nanoparticles and nanocubes were investigated by XRD and the resulting peaks were matched to hexagonal zinc oxide phase as shown in **(Figure 5 -7)**.

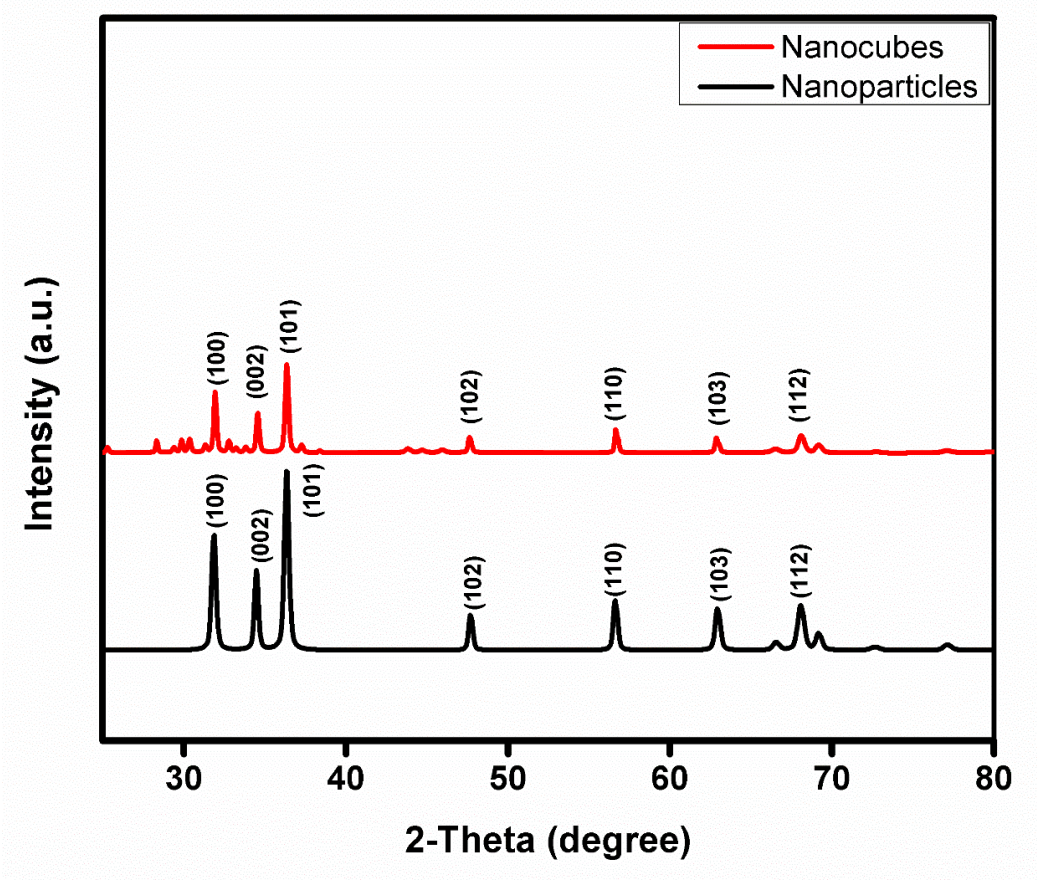

Figure 5 - 7: XRD peaks for Zinc oxide nanoparticles and nanocubes.

Through the XRD analysis and looking at different intensities the following has been observed. Although peaks are identical due to identical chemical compositions each peak has a different intensity. This is can be attributed to the difference of preferential growth face of the crystal resulting in the different face area of crystal. The highest intensity is at (101) which is the preferential growth face.

The XRD calculations using Bragg's law takes into account some assumptions that never happen in actual cases. The assumptions are that the beam analyzing the crystal is perfectly parallel and monochromatic and that the crystal is perfect. Thus, it is worth mentioning that such imperfections affect the broadening of the XRD peaks as well as other factors. There are mainly three factors that affect the broadening of the diffraction peaks including instrumental effects, arising from imperfect focusing, crystallite size, and lattice strain. Thus, it is possible to quantitatively evaluate the effect of micro-strain as well as crystallite size using Scherrer equation. It is shown in **(Table 5 – 2)** the raw data acquired by XRD of the selected zinc oxide nanostructures matched to their miller indices through hexagonal zinc oxide phase. Using the highest intensity peak other parameters (crystallite size, strain, and poly-dispersity) were calculated using Scherrer equation.

Table 5 - 2: Raw XRD data with matched miller indices based on hexagonal phase.

Zinc oxide nanoparticles				
Pos. [°2Th.]	Height [cts]	Miller indices	d-spacing [Å]	Rel. Int. [%]
31.8311	454.86	(100)	2.81138	62.66
34.4562	327.01	(002)	2.60296	45.05
36.3203	725.89	(101)	2.47353	100
47.6632	153.95	(102)	1.90802	21.21
56.5901	229.88	(110)	1.62641	31.67
62.8938	189.45	(103)	1.47772	26.1
66.4966	33.28	(200)	1.40613	4.59
68.023	192.49	(112)	1.37825	26.52
69.1243	71.8	(201)	1.35896	9.89
72.5949	13.19	(004)	1.30231	1.82
77.0504	23.16	(202)	1.23774	3.19
Zinc oxide nanocubes				
Pos. [°2Th.]	Height [cts]	Miller indices	d-spacing [Å]	Rel. Int. [%]
31.8554	183.37	(100)	2.80929	5.23
34.534	183.39	(002)	2.59728	5.23
36.3344	345.16	(101)	2.47261	9.84
47.599	79.05	(102)	1.91045	2.25
56.6993	87.42	(110)	1.62353	2.49
62.9699	88.66	(103)	1.47612	2.53
68.0511	67.79	(112)	1.37775	1.93
77.021	9.9	(202)	1.23814	0.28

In order to calculate crystallite size, strain and polydispersity; Scherrer equation is used and the resulting data has been presented in **(Table 5-3)**.

$$D_p = \frac{K \times \lambda}{\beta_{\frac{1}{2}} \times \cos(\theta)} \qquad \text{[Equation 5.1]}$$

where D_p = crystallite size, K = constant of 0.94, β = Line broadening in radians, θ = Bragg angle, and λ = X-ray wavelength.

$$\eta = \frac{\beta_{Strain}}{\tan(\theta)} \qquad \text{[Equation 5.2]}$$

Where η is the strain, β_{Strain}= broadening due to strain, and θ = Bragg's angle

$$\rho = \frac{\sigma}{d} \qquad \text{[Equation 5.3]}$$

where ρ is the degree of poly-dispersity, σ is the standard deviation of crystal-size, and d is the mean crystal-size. Usually small ρ indicates a uniform size distribution.

Table 5 - 3: Crystallite size, Strain, poly-dispersity calculation.

ZnO nanostructure	Position (2 theta) degrees	FWHM (degrees)	Crystallite size (nm)	Strain (%)	Poly-dispersity (%)
Nanoparticles	36.3	0.2952	29.59	0.39	23
Nanocubes	36.3	0.2066	42.28	0.27	20

5.4. XPS analysis:

The analysis used in XPS are shown in **(Figure 5-8)**, it presents the XPS core spectra recorded for O1s and Zn 2p. XPS was performed for ZnO in all its forms to study the chemical states as well was the binding energies of both the Zn and O, by which it can help to interpret the TGA results. Zn 2p spectra of the NCs are shown in Figure 4.b where doublet peak can clearly be seen at 1024.5 eV and 1047.6 eV corresponding to Zn 2p 3/2 and Zn 2p ½, respectively. A spin-orbit splitting of 23.1 eV between the two peaks confirms that the Zn is in Zn2+ state. The O1s peak of the NCs showed a tail towards higher

binding energies. Those peaks were carefully deconvoluted into 2 symmetric peaks **(Figure 5-9)**, a sharp peak at 533.2 eV which can be attributed to the intrinsic lattice oxygen in the wurtzite ZnO lattice, and a smaller peak at a higher binding (534.8 eV) which corresponds to the loosely bound oxygen on the surface in the form of OH.

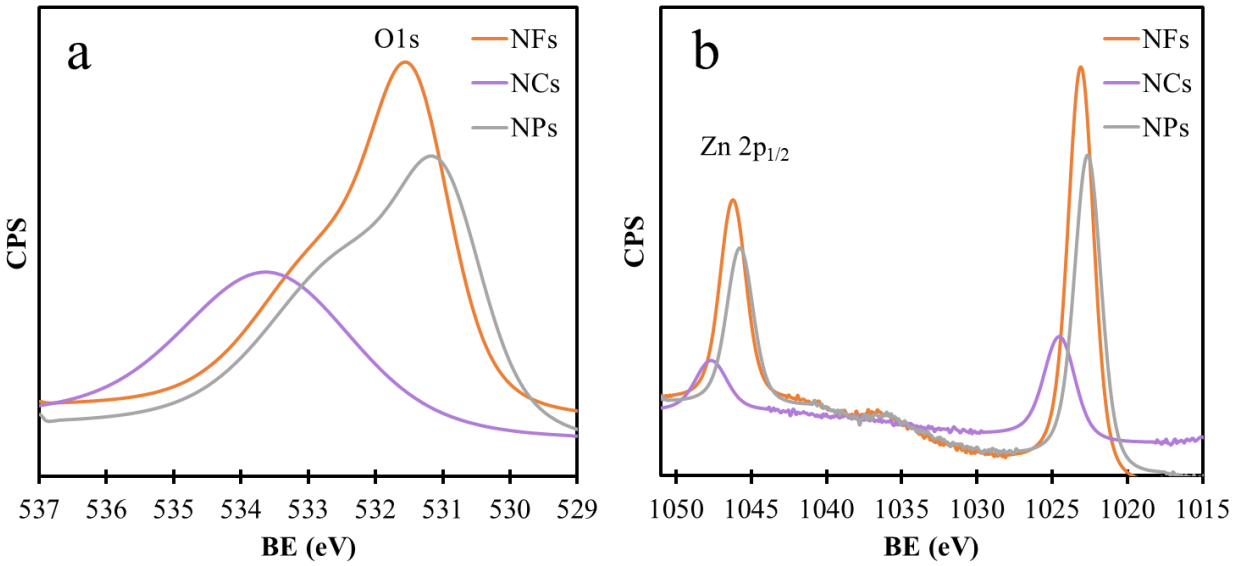

Figure 5 - 8: XPS core level spectra of (a) O1s and (b) Zn 2p.

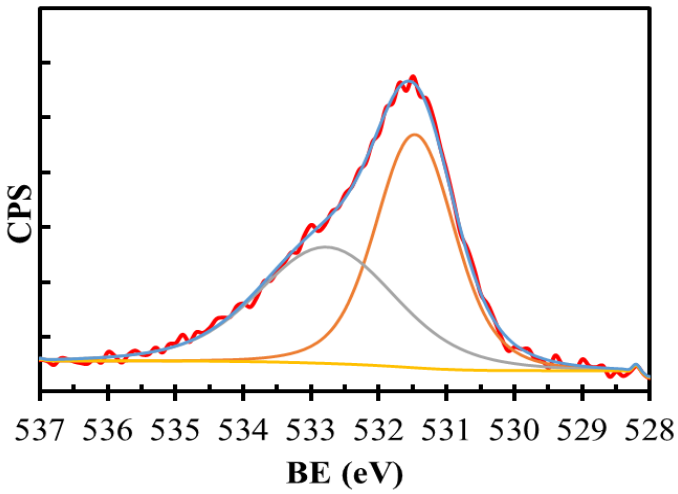

Figure 5 - 9: O1s peak of the NCs

The analysis of O1s peak representing the contribution of oxygen in the hydroxyl groups are shown in **(Figure 5-10)** shows the ratio between the oxygen in the OH form and the total oxygen in the samples. It can clearly be seen that the OH contribution in the NCs is the least compared to the NPs and NFs, which can explain the difference in their performance upon conducting the TGA test. TGA results can be interpreted in terms of geometry, as the NCs have higher surface area to volume ratio compared to the other two structures. In addition, NCs possess at least 12 sharp edges, while NFs and NPs have none. Hence, the largest number of dangling bonds and active surface sites can be found in the NCs. Besides, the O1s peak of the NCs had the least OH contribution in the O1s peak, leaving a room for the rest of the dangling bonds to interact with the polymer. This enhanced ZnO-polymer interaction kept the polymer from degradation. Thus, NCs showed the least weight loss compared to the NFs and NPs.

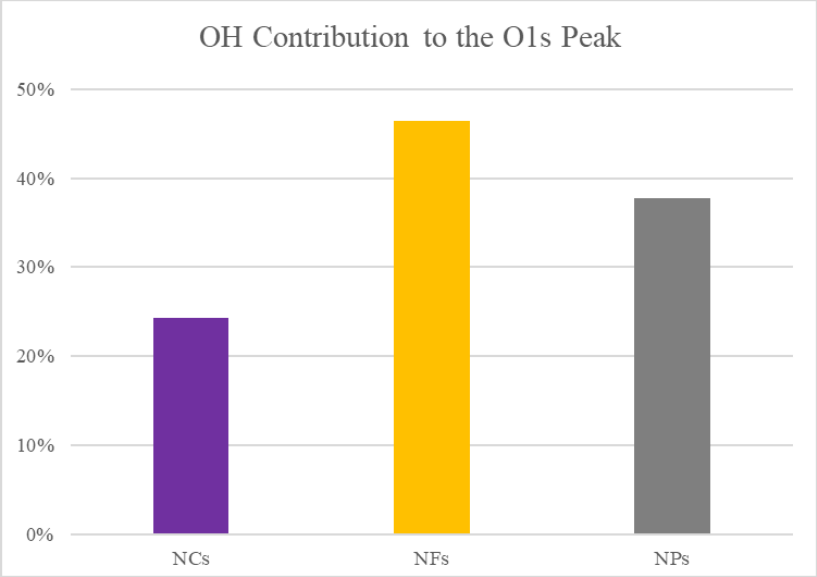

Figure 5 - 10: OH ratios in O1s peaks.

5.5. Polyacrylamide Water uptake:

The water uptake test showed a very high absorption of polyacrylamide polymer to water. It proved absorption of more than 300 %. This proves the high efficiency of PAM polymer used in further tests.

5.6. Polyacrylamide Rheology tests:

The selected zinc oxide nanostructures were mixed with polymers and were tested for viscosity and surface tension and were compared to polymer only. The surface tension was measured as an indication of interfacial tension. As a primary comparison blank polymer was compared to nano + PAM polymer at room temperature and zero salinity. The results were tabulated in **(Table 5-4)** and the viscosity results were graphically represented at different shear rates.

Table 5 - 4: Comparison between blank PAM and nano + PAM at 0 NaCl, room temp., and 600 rpm.

	Concentration (wt %)	Density (g/cm3)	S. Tension (N/m)	pH	Viscosity (cP)
	0	1.018	108.89	6.45	38
NPs	0.5	1.011	136.87	7.07	37
	3	1.02	140.13	7.53	37
NCs	0.5	1.026	141.13	7.36	32
	3	1.039	134.94	7.28	35

The results in **(Table 5-4)** shows the bad effect of Zinc oxide nanoparticles and nanocubes on PAM polymer. It is more favorable for oil recovery to have less surface tension and higher viscosity. To make sure that the results presented previously especially for viscosity, it was necessary to check the viscosity results at different shear rates. The results of viscosity at different shear rates were shown at **(Table 5-5)**.

Table 5 - 5: Effect of different nanoparticle concentrations on PAM at different shear rates, zero salinity, and room temperature.

0 % Salinity and room temperature									
0 Nano		0.5 NPs		3 NPs		0.5 NCs		3 NCs	
shear rate (rpm)	Viscosity (cP)	shear rate (rpm)	Viscosity (cP)	shear rate (rpm)	Viscosity (cP)	shear rate (rpm)	Viscosity (cP)	shear rate (rpm)	Viscosity (cP)
30	170	30	130	30	150	30	110	30	140
60	125	60	85	60	90	60	80	60	85
100	96	100	78	100	81	100	66	100	72
200	69	200	57	200	57	200	51	200	55.5
300	54	300	49	300	49	300	43	300	48
600	38	600	37	600	37	600	32	600	36

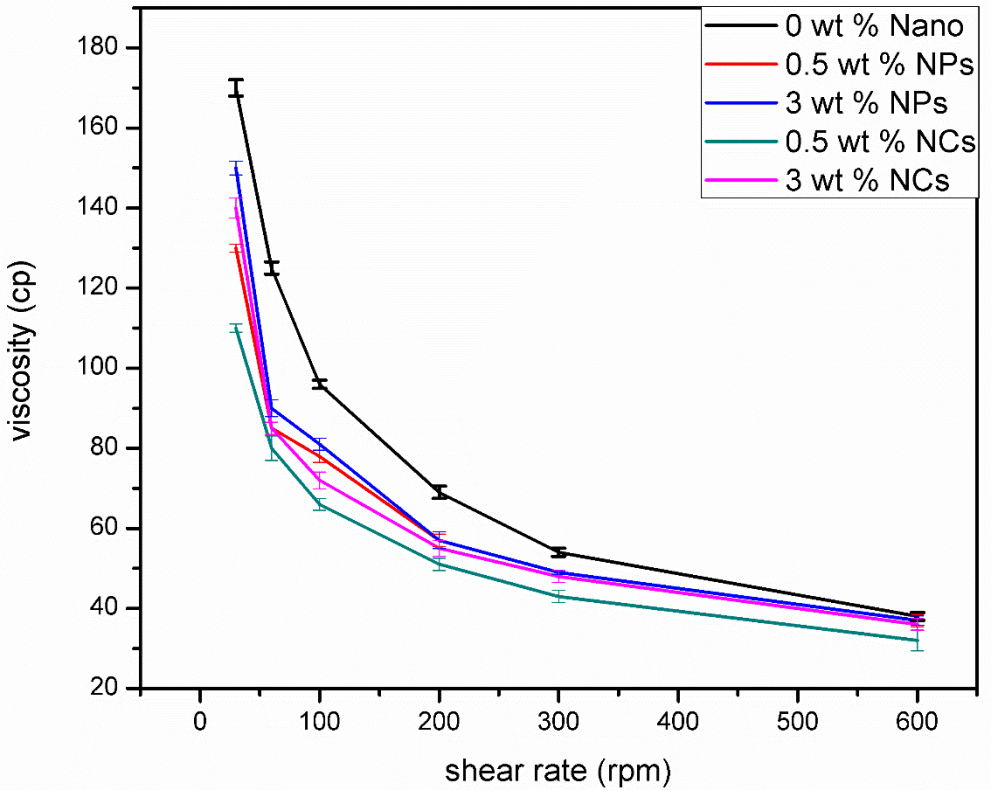

Figure 5 - 11: Effect of Nanoparticles concentrations on PAM polymer at different shear rates.

5.7. Guar gum polymer TGA

A comparison was made within each structure and between different structures to reach the optimum concentration for the nanocomposites. Since not all films had the same weight before going into thermogravimetric analysis; the comparison was based on weight percent reduction. In other words, the less the weight reduction is the better the polymer stability and hence more cost effective during polymer flooding operation. The interval for calculating the weight loss reduction is between 300 ^{0}C and 350 ^{0}C since it is the interval in which the polymer starts degradation. According to **(Figure 5 - 12 a, b, and c)**, shows the optimum concentration for ZnO nanostructures used in nanocomposites. The results showed that 3% ZnO was the optimum for both nanocubes and nanofibers while the optimum concentration for the nanoparticles was 0.5 %. When such concentrations were compared to the pure polymer as in **(Figure 5 - 12 d)**; it showed that 3% nanocubes is the best nanocomposite leading to the least weight loss in the polymer. The higher thermal stability of the nanocubes composite could be attributed to its unique crystallographic planes. Such planes are exposed to the outside allowing more interaction with the polymer and supporting high surface to volume ratio that enhances the reactivity compared to the other structures. Interestingly, although 3% nanocubes composite showed the best results, only 0.5% of the nanoparticles composite showed enhancement in the stability compared to the pure polymers well. In other words, if the usage of different nanostructures would be implemented in the industry; it would need further financial feasibility to decide whether using more percentage of nanostructures to enhance the polymer's stability would pay off for the economics or not.

TGA results can be interpreted in terms of geometry, as the NCs has higher surface area to volume ratio compared to the other two structures. In addition, NCs possess at least 12 sharp edges, while NFs and NPs have none. Hence, the largest number of dangling bonds and active surface sites can be found in the NCs. Besides, the O1s peak of the NCs had the least OH contribution in the O1s peak, leaving a room for the rest of the dangling bonds to interact with the polymer. This enhanced ZnO-polymer

interaction kept the polymer from degradation. Thus, NCs showed the least weight loss compared to the NFs and NPs.

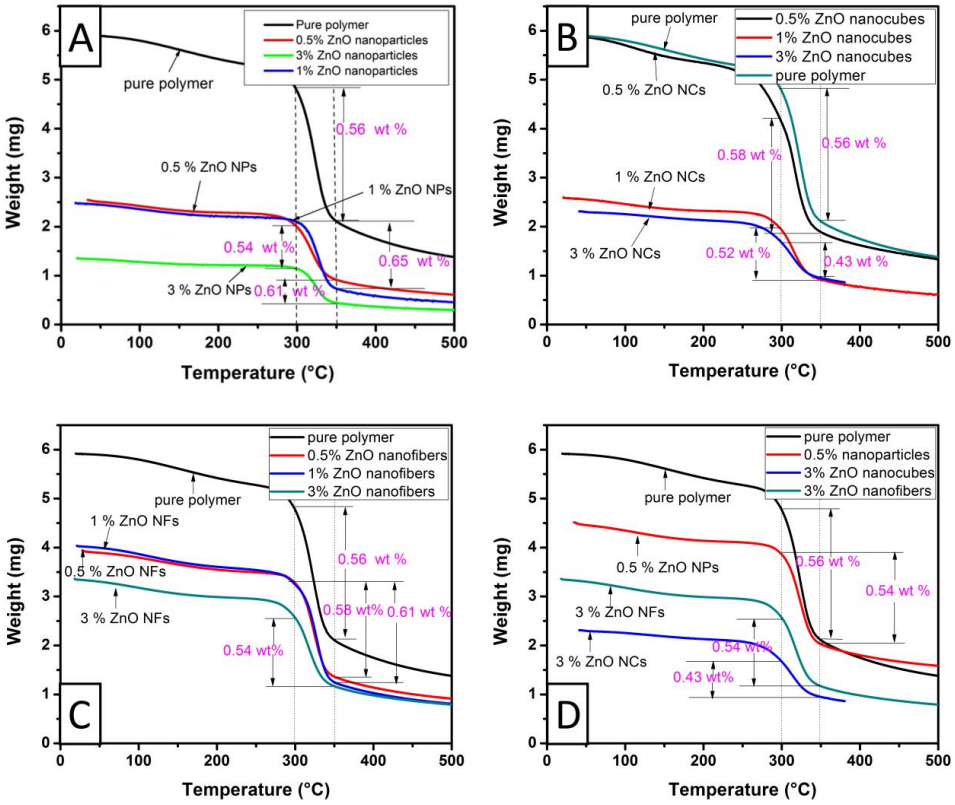

Figure 5 - 12: TGA of Guar gum/ZnO nanocomposites.

5.8. Nanofluids stability

The stability tests for polymers, anionic and cationic surfactants were made by spectrophotometer at a wavelength of 360 nm. The wavelength used was less than the final one used since the main idea behind the first tests was not to compare but to get an idea of the general stability behavior of different fluids. ZnO suspensions in DIW wasn't measured quantitatively by spectrophotometer because they precipitated in less than 24 hours. The first thing to evaluate based on the previous chapter is the difference in stability between nanoparticles suspensions in PAM at pH of 8.5 versus PAM at pH 12. The results were tabulated in **(Table 5-6)** and graphically represented at **(Figure 5-13)**.

Table 5 - 6: Effect of PAM polymer on ZnO suspensions.

Fluid type	0 hour	1 hour	2 hours	3 hours	4 hours
PAM, 0.05 NP, pH8.5	0.858	0.833	0.858	0.633	0.598
PAM, 0.1 NP, pH8.5	1.588	1.575	1.255	1.184	1.079
PAM, 0.2 NP, pH8.5	3.8	2.349	1.842	1.8	1.725
PAM, 0.3 NP, pH8.5	3.8	2.07	1.302	1.191	0.645
PAM, 0.05 NP, pH12	0.836	0.823	0.823	0.823	0.77
PAM, 0.1 NP, pH12	1.559	1.482	0.863	0.863	0.81
PAM, 0.2 NP, pH12	0.734	0.722	0.676	0.536	0.518
PAM, 0.3 NP, pH12	1.052	0.885	0.633	0.557	0.392

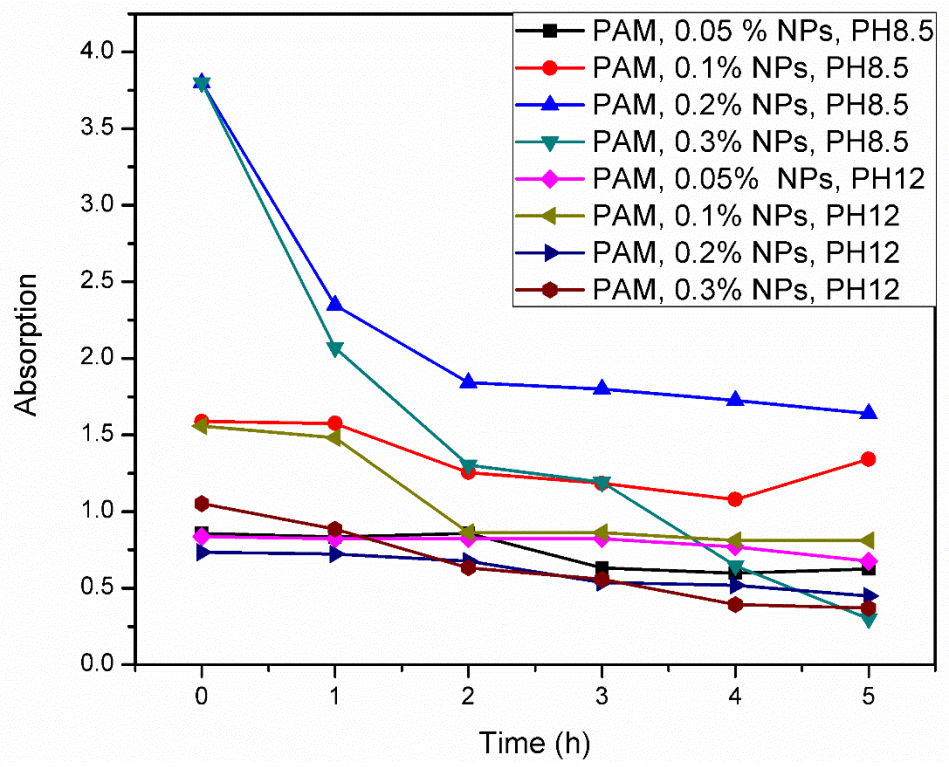

Figure 5 - 13: Slopes comparison of different PAM suspensions.

The results above shown in **(Figure 5-13)** show that the polymer is extremely unstable except in the nanoparticles concentration of 0.05 and 0.1 at pH 12. However, the visual observation showed that the most stable suspensions precipitated after 36 hours only as shown in **(Figure 5-**

14).

Figure 5 - 14: (a) PAM+ ZnO suspensions right after sonication - (b) PAM + ZnO suspensions after 36 hours.

Next thing, it was essential to assess the effect of both anionic and cationic surfactants on the stability of zinc oxide nanoparticles. The concentrations of the SDBS and CTAB were selected based on literature and CMC. Two concentrations of SDBS were selected (CMC and above CMC) and the suspension was set on pH 7.7 since suspensions of ZnO ready-made at manufacturers are stable around this pH. However, since CTAB was used only at CMC concentration; it was investigated at basic pH (12) as well as normal (7.7). The results of the stability measurements of anionic surfactants and cationic surfactants were tabulated and represented graphically in **(Table 5 - 7)**, **(Table 5 - 8)** and **(Figure 5 - 15)**, **(Figure 5 - 16)** respectively.

Table 5 - 6: Effect of anionic surfactant on ZnO suspensions.

	Absorbance - Vs Time (hours)		
Suspension Label	0 hour	1 hour	2 hours
0.025 SDBS, 0.05 NP, pH 7.7	1.23	1.305	1.155
0.025 SDBS, 0.1 NP, pH 7.7	1.364	2.147	2.068
0.025 SDBS, 0.2 NP, pH 7.7	2.3	1.984	1.853
0.017 SDBS, 0.05 NP, pH 7.7	1.23	1.134	1.119
0.017 SDBS, 0.1 NP, pH 7.7	1.364	2.181	1.679
0.017 SDBS, 0.2 NP, pH 7.7	2.3	0.177	0.103

Table 5 - 7: Effect of cationic surfactant on ZnO suspensions data.

	Absorbance - Vs Time (hours)	
Suspension Label	0 hour	1 hour
0.0146 CTAB, 0.05 NP, pH 12	1.53	1.26
0.0146 CTAB, 0.1 NP, pH 12	0.636	0.42
0.0146 CTAB, 0.2 NP, pH 12	0.63	0.16
0.0146 CTAB, 0.05 NP, pH 7.7	0.437	0.117
0.0146 CTAB, 0.1 NP, pH 7.7	0.839	0.163
0.0146 CTAB, 0.2 NP, pH 7.7	0.705	0.153

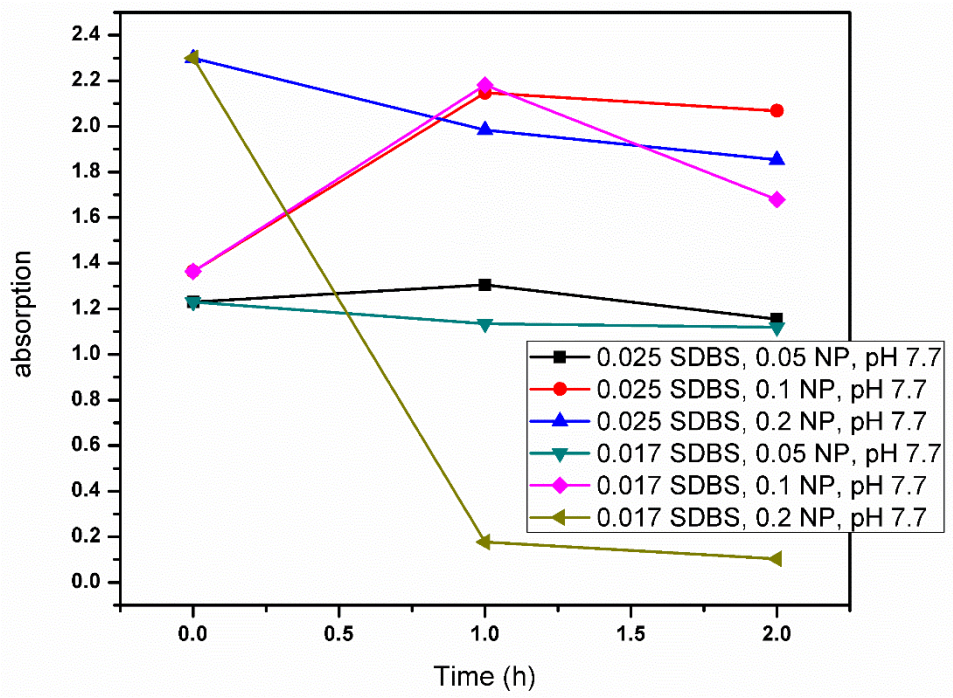

Figure 5 - 15: Effect of different concentrations of SDBS anionic surfactant on ZnO suspensions' stability.

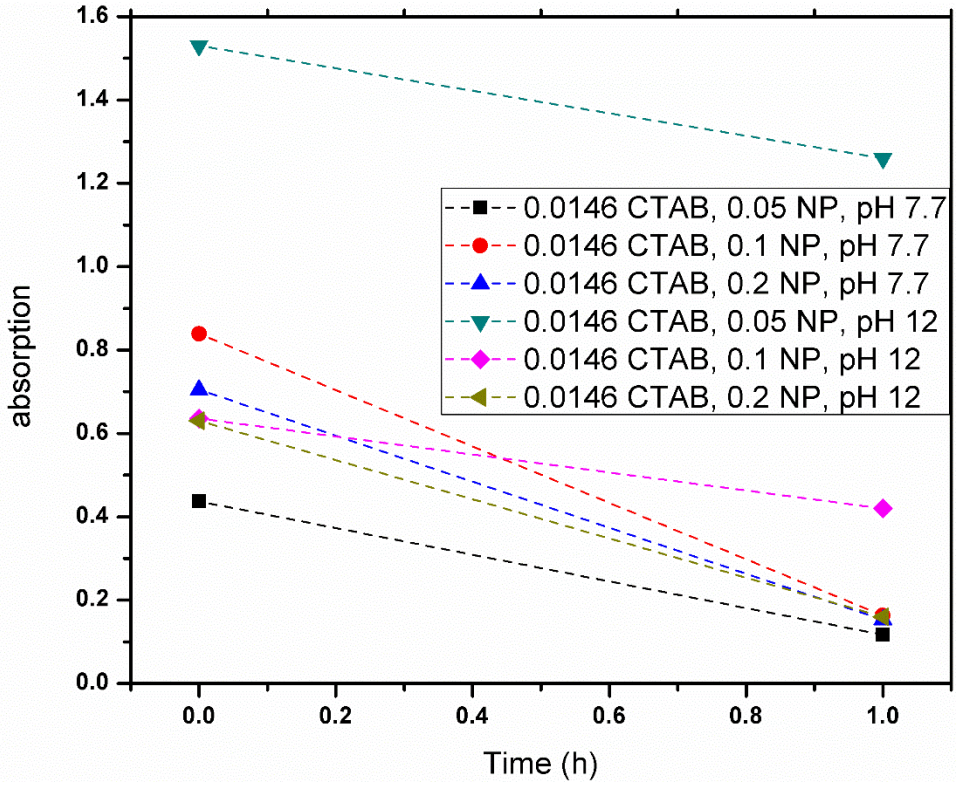

Figure 5 - 16: different concentrations of CTAB cationic surfactant on ZnO suspensions' stability.

The results of the previous graphs and tables ensure only a few things. Firstly, from the slopes of different pHs of different concentrations of ZnO nanoparticles suspension in CTAB; it can prove that CTAB is not as stable as SDBS surfactant. In other words, anionic surfactants keep the suspension stable for longer periods of time compared to cationic surfactant. Secondly, the most stable nanoparticles concentrations are 0.05 and 0.1 weight percent while 0.2 weight percent proved to precipitate faster than others. Finally, it has been shown that anionic surfactant SDBS was able to be relatively stable in both pHs 7.7 and 12. The observations drawn from the previous step initiated one more stability test for the most stable SDBS surfactants. The results of such test were tabulated at **(Table 5 - 9)** and graphically represented in **(Figure 5 - 17)**.

Table 5 - 8: Most stable concentrations of SDBS surfactants at the most stable nanoparticles concentrations.

Suspension Label	Absorbance - Vs Time (hours)			
	0 hour	1 hour	2 hours	3 hours
0.025% SDBS, 0.1 NP, pH7.7	1.951	1.927	1.874	1.817
0.025% SDBS, 0.05 NP, pH7.7	1.125	1.096	1.076	1.044
0.017% SDBS, 0.05 NP, pH7.7	1.035	1.004	0.986	0.95
0.2% SDS, 0.05 NP, pH7.7	1.281	1.258	1.217	1.109
0.2% SDS, 0.1 NP, pH7.7	2.136	2.077	1.944	1.853

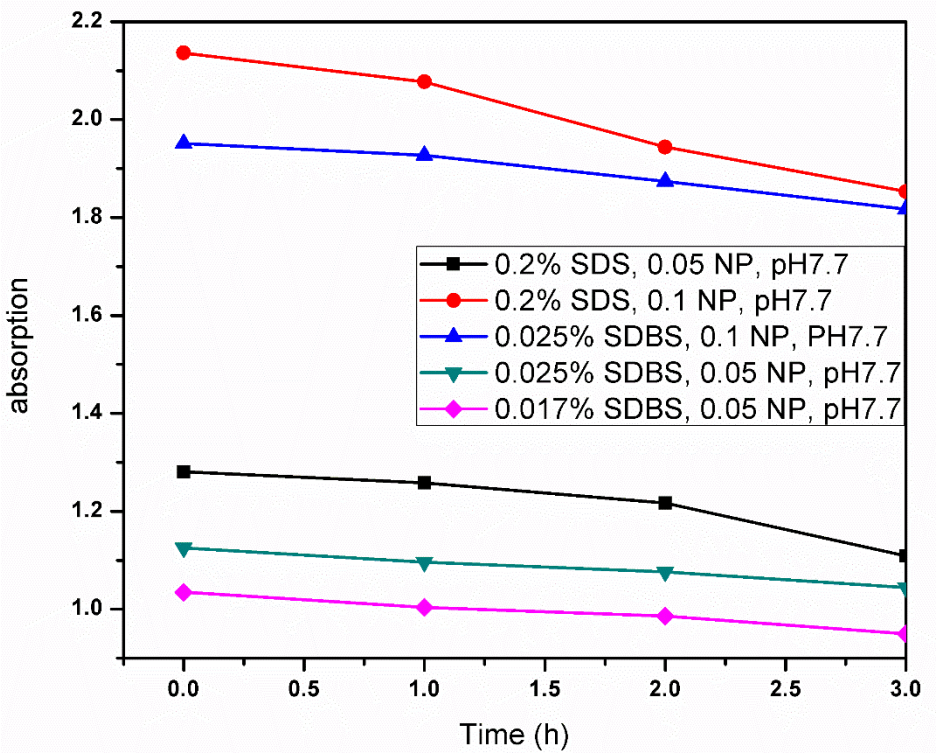

Figure 5 - 17: Most stable SDBS surfactant concentrations at most stable NPs concentrations.

It was proven from **(Figure 5 - 17)** the huge difference in the stability through the difference of slope compared to **(Figure 5 - 15)**. Thus, it was necessary to check the effect of nanoparticles when suspended in SDBS surfactant on interfacial tension versus n-dodecane. The results of the IFT measurements for such experiment were tabulated and graphically represented in **(Table 5-10)** and **(Figure 5 - 18)**.

Table 5 - 9: IFT measurements for selected SDBS concentrations and selected NPs concentrations.

Fluid type	Concentration (weight percent)	IFT (mN/m)
Surfactant only	0	43.1
	0.0056	17.2
	0.0113	13.2
	0.017	10.9
	0.023	10.7
	0.028	8.7
0.017 SDBS, NPs	0	10.9
	0.05	8.5
	0.1	9.6
	0.2	13
0.023 SDBS, NPs	0	10.8
	0.05	9.3
	0.1	9.7
	0.2	9.8

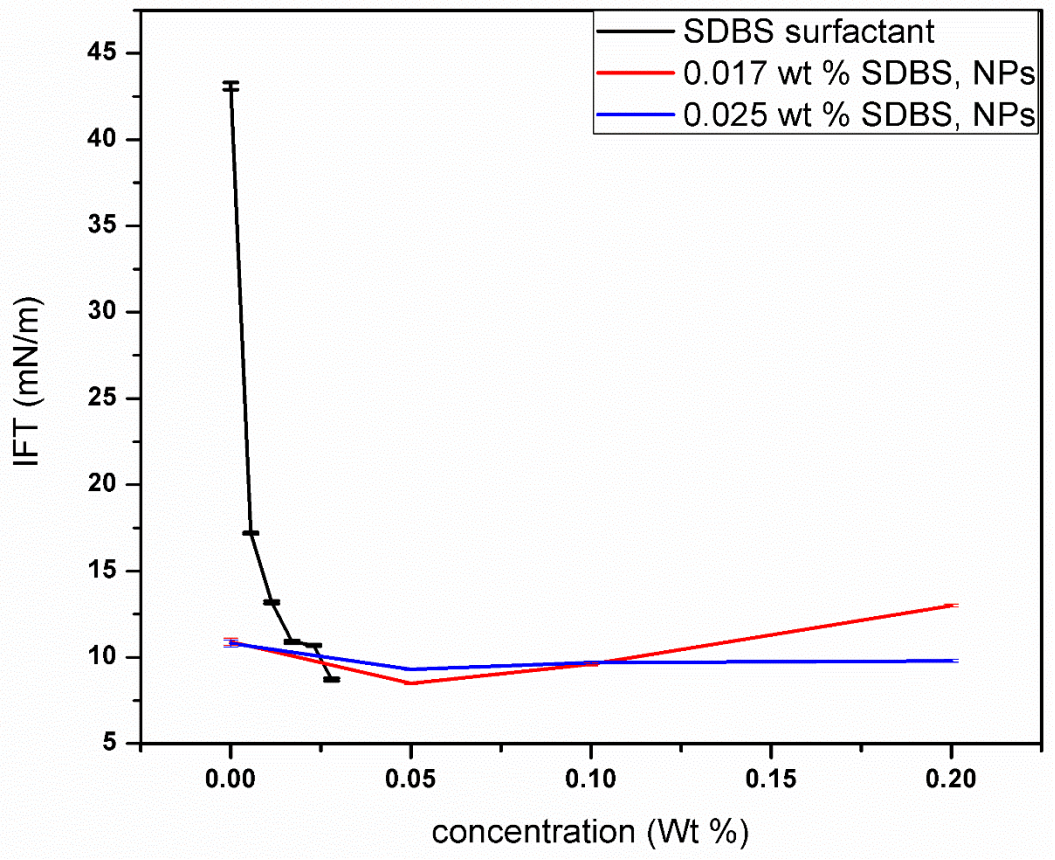

Figure 5 - 18: IFT measurements of SDBS surfactants compared to SDBS + NPs suspensions.

The interfacial tension measurements proved that the least IFT can be reached by SDBS which is 8.8 mN/m2 wasn't reduced much by the effect of adding ZnO nanoparticles. Therefore, it will be uneconomical to use it for field scale projects and there will be no sense to add it in core flood system since it will not increase the oil recovery. Subsequently, it was essential to run same tests on a different anionic surfactant (SDS). The SDS was tested for stability as well as IFT measurements at 0.2 weight percent (CMC) and pH 8.4. The stability measurements were evaluated quantitatively for 26 hours and observed visually afterward since it totally stabilized even quantitatively. The results are tabulated in **(Table 5 - 11)**, **(Table 5 - 12)** and **(Figure 5 - 19), (Figure 5 - 20)**.

Table 5 - 10: Stability measurements for ZnO suspensions in 0.2 wt % SDS surfactant.

Suspension Label	0	1	2	18	19	20	21	22	23	24	25	26
0.2 % SDS, 0.05 NP	0.44	0.417	0.394	0.134	0.111	0.111	0.107	0.097	0.084	0.083	0.083	0.083
0.2 % SDS, 0.1 NP	0.887	0.804	0.726	0.169	0.15	0.148	0.148	0.149	0.148	0.148	0.148	0.148
0.2 % SDS, 0.2 NP	1.83	1.739	1.672	0.466	0.453	0.452	0.449	0.448	0.445	0.445	0.445	0.455

Table 5 - 11: IFT measurements for ZnO suspensions in 0.2 wt % SDS surfactant.

NPs conc.	Sample	IFT 1	IFT 2	IFT 3	IFT
0	0.2 % SDS	32.5	32.2	32.7	32.5
0.05	0.2 % SDS, 0.05 NP	7	7.1	7.1	7.1
0.1	0.2 % SDS, 0.1 NP	8	8.1	8.2	8.1
0.2	0.2 % SDS, 0.2 NP	8	8.2	8.1	8.1

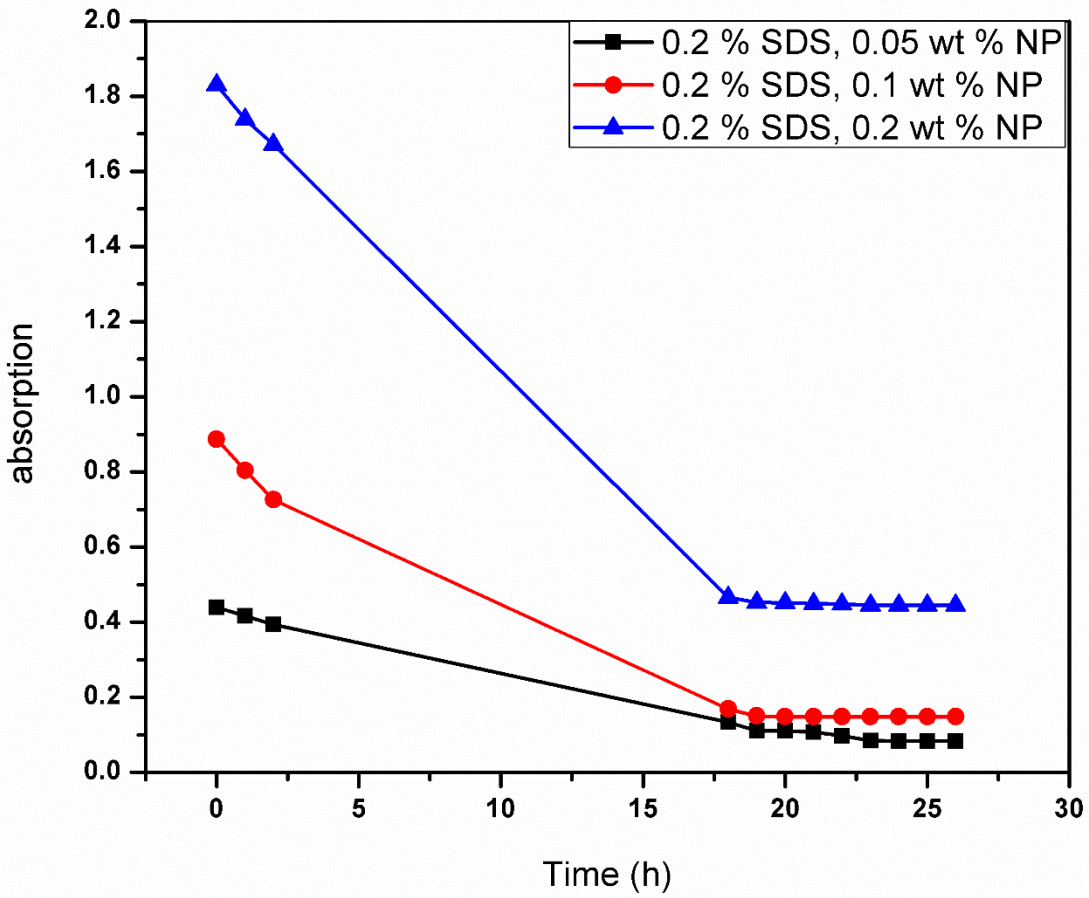

Figure 5 - 19: Stability measurements of ZnO NPs suspensions in SDS surfactant.

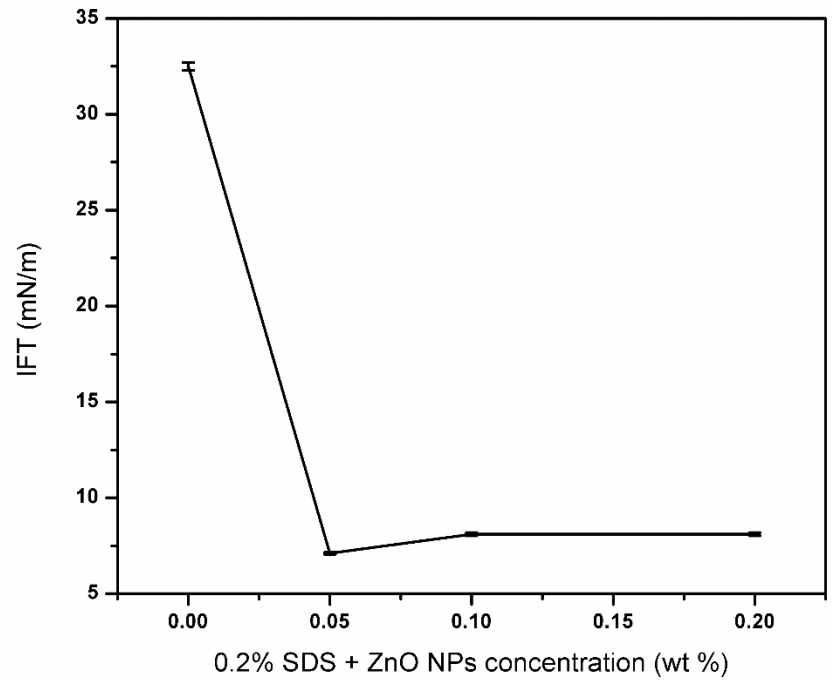

Figure 5 - 20: Stability measurements of ZnO NPs suspensions in 0.2 wt % SDS surfactant.

It can be observed from the previous two tables and figures that ZnO suspensions in SDS can be stable as long as SDBS surfactant. In addition, IFT measurements showed that ZnO NPs suspension in SDS surfactant can hugely reduce IFT versus n- dodecane compared to pure SDS versus n-dodecane. Hence, 0.1 % NPs suspended in 0.2 weight percent SDS surfactant was selected to be used for core flooding experiments.

5.9. Core flooding

The results of sandstone core SEM and EDX are shown in **(Figure 5 - 21)**

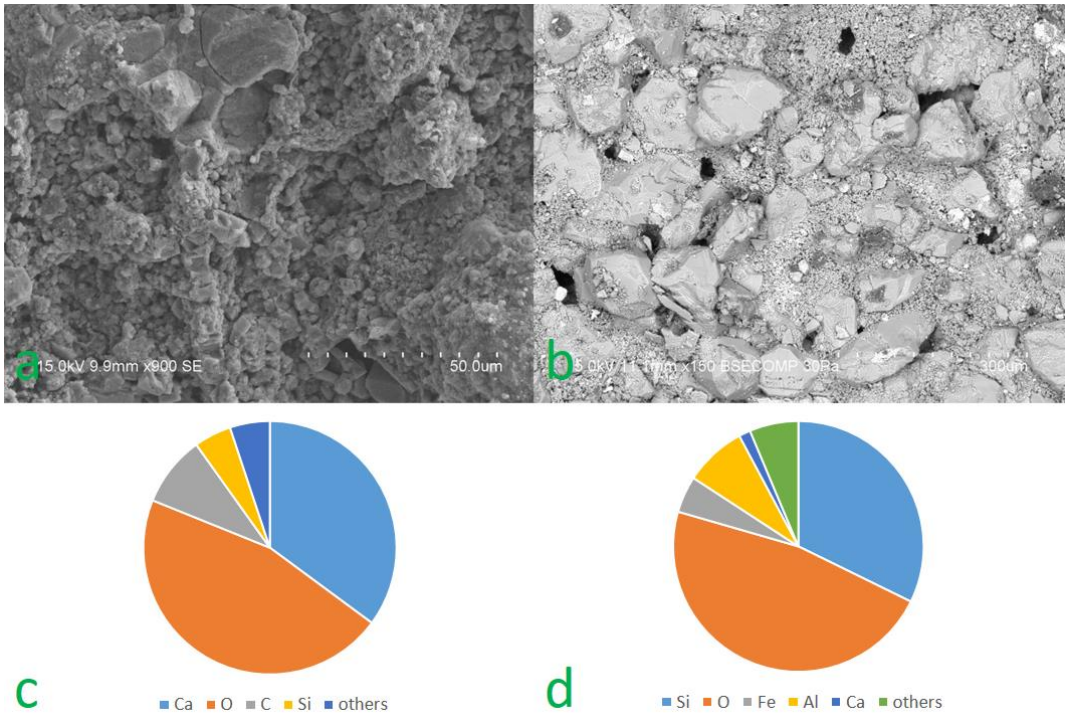

Figure 5 - 21: (a) SEM of limestone. (b) SEM of sandstone. (c) EDX of limestone. (d) EDX of sandstone.

The SEM images show the extreme difference in porosity between the limestone samples and the sandstone sample. Even through running permeability test for limestone; the core sample got fractured out of pressure due to the pressure differential between inlet and outlet. The sample showed very little amount of DIW produced in comparison to what is being injected.

As mentioned in chapter 4, brief details were mentioned about the general scheme in which the core flooding experiment is executed. The experiment started by measuring the absolute

permeability of carbonate rocks which hasn't been used eventually. It showed extremely low permeability which can be discovered by the increase in differential pressure due to the high difference between the inlet and outlet pressure. Therefore, the sandstone samples were used instead. During run 1, the first sandstone core sample (MS1) was used for surfactant flooding with no ZnO nanoparticles at all. During run 2, the second sandstone core sample (MS2) was used for ZnO nanoparticles surfactant flooding. As for run 3, which includes ZnO nanocubes surfactant flooding, wasn't executed due to the very close results obtained from interfacial tension measurements from nanocubes compared to nanoparticles. The details of the absolute permeability measurements of the core samples used in the flooding experiments were tabulated and graphically represented in **(Table 5 - 13)** and **(Figure 5 - 22)**.

Table 5 - 12: details of the core samples used in the flooding experiments.

Core ID:	MS1	MS2
Diameter (cm):	2.52	2.52
Length (cm):	6.72	6.67
Surface (cm^2):	4.99	4.99
Volume(cc):	33.52	33.27
Pore Vol. (ml):	8.89	8.87
Porosity (%):	26.51	26.65
Absolute permeability (md)	28.137	15.745

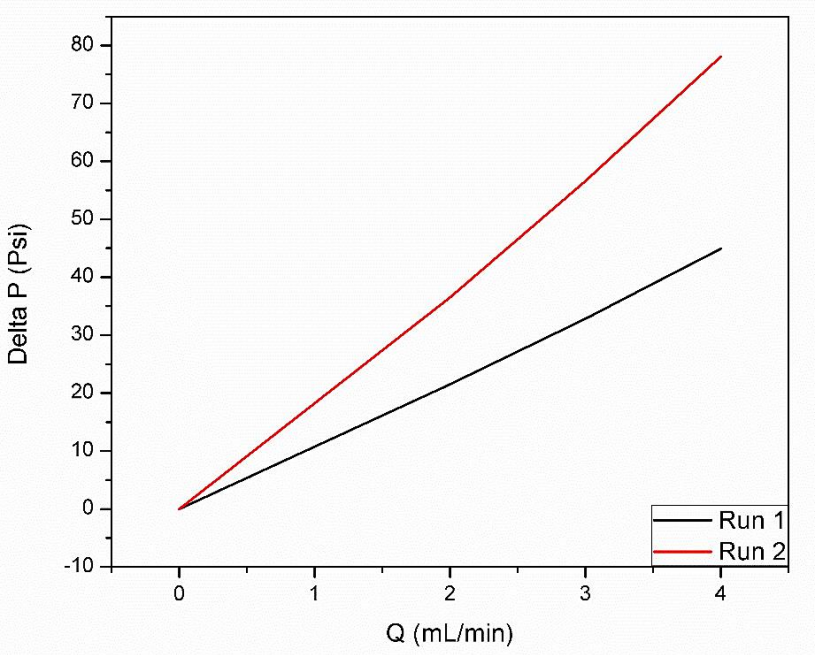

Figure 5 - 22: diffrential pressure profile for absolute permeability measurements.

The higher differential pressure observed in run 2 with core (MS 2) could be attributed to the less absolute permeability calculated and mentioned in **(Table 5 - 13)**. The reduction in absolute permeability causes less produced fluids at the same rate used for both core samples. Thus, more pressure build-up can be observed at the outlet where fluids are produced. The results for the core samples used can be presented in terms of three main processes including absolute permeability measurement shown previously, saturation profile at water flooding (WF), and saturation profile at tertiary recovery (surfactant flooding for MS1, ZnO NPs/surfactant flooding for MS2). The details of the experiments done are shown in **(Table 5 - 14)** and the saturation profiles are shown in **(Figure 5-23)**.

Table 5 - 13: Flooding processes details.

	Process	Sw (%)	So (%)	SWc	Sor	q (cc/min)	$PV_{injected}$ (ml)
Run 1 (MS1)	Water	100	NA	NA	NA	2, 3, 4	8.89
	Oil	32.5	67.5	32.5	NA	0.5, 1	4PV+0.9 PV = 44.5
	Water	66.25	33.75	32.5	NA	0.5	5 PV = 44.45
	Surfactant	71.87	28.13	32.5	28.13	0.5	6 PV = 53.34
Run 2 (MS2)	Water	100	NA	NA	NA	2, 3, 4	8.87
	Oil	29	71	29	NA	0.5, 1, 2	4PV
	Water	60.6	39.4	29	NA	0.5	5 PV
	NPs/SDS	74.1	25.9	29	25.9	0.5	6 PV+ 2 PV (still producing)

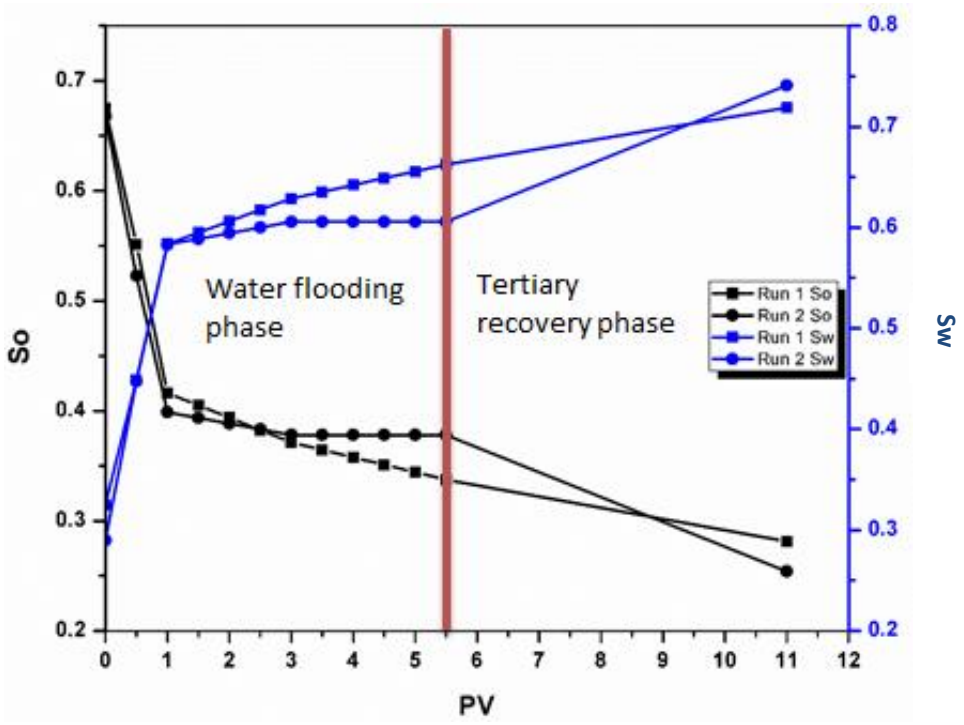

Figure 5 - 23: Saturation profiles for run 1 (SDS) flooding, and run 2 (NPs/SDS) flooding.

The representation of the saturation profile of the flooding processes presented in **(Figure 5 – 23) (Table 5 – 14)**. Initially, at 0 PV displacement, the oil and water initial saturations were presented after injecting them in the core sample. Later, the first 5.5 PV represents the water flooding phase where no more significant oil was produced by its end. The endpoints of saturation were presented by the final amount of residual oil saturation and water saturation. This case wasn't having enough points as in water flooding phase due to the relatively little amount of oil produced at each half pore volume. Generally speaking, it was confirmed from **(Table 5 – 14)** and **(Figure 5 – 23)**; that the residual oil saturation in surfactant (SDS) flooding was much higher than ZnO/SDS flooding. In other words, although NPs/SDS flooding started with a higher oil saturation after water flooding but it was possible to show less residual oil saturation by the end of tertiary phase compared to conventional surfactant flooding.

References:

1) Antony, R. P.; Mathews, T.; Dasgupta, A.; Dash, S.; Tyagi, A.; Raj, B. Rapid breakdown anodization technique for the synthesis of high aspect ratio and high surface area anatase TiO_2 nanotube powders. *Journal of Solid State Chemistry* **2011**, *184*, 624–632.
2) Nakayama, K.; Kubo, T.; Nishikitani, Y. Anodic Formation of Titania Nanotubes with Ultrahigh Aspect Ratio. *Electrochemical and Solid-State Letters* **2008**, *11*.
3) Ali, S.; Hannula, S.-P. Titania nanotube powders obtained by rapid breakdown anodization in perchloric acid electrolytes. *Journal of Solid State Chemistry* **2017**, *249*, 189–198.

Chapter 6

Conclusions and Future Work

Based on the work presented in chapter 4 and 5, the below conclusions could be stated:

1- It was possible to show the growth mechanism of zinc oxide from rods to flowers. This can give some potential for more optimization of this work to produce the mentioned structures with more uniformity and a good size to be used in various applications.

2- It was concluded that zinc oxide has a negative effect on polyacrylamide due to the exacerbation of its viscoelastic properties at room conditions.

3- Zinc oxide nanocubes had an enhancement effect on guar gum polymer which was indicated by both TGA and XPS compared to zinc oxide nanoparticles and annealed nanofibers.

4- Zinc oxide NCs' enhancement for guar gum's thermal stability was attributed to excess dangling bonds resulting from less chemisorbed OH groups on its surface compared to other nanostructures

5- Different morphologies of zinc oxide showed no significant difference in interfacial tension measurements which may conclude that they wouldn't show difference in oil recovery.

6- ZnO NPs exhibited good suspension stability in SDS compared to other anionic and cationic surfactants or water.

7- Core flood experiments proved that ZnO NPs/SDS flooding can be very useful to increase the amount of oil recovered from sandstone formation

8- Upon proving that zinc oxide nanoparticles have a good potential to be used in oil recovery, more work can be done to test other metal oxides with their different nanostructures like titanium dioxide.